Macromolecular crystallization in microgravity

Edward H Snell[1] **and John R Helliwell**[2,3]

[1] Biophysics Group, NASA Marshall Space Flight Center, Code XD42, Huntsville, AL 35812, USA
[2] Department of Chemistry, The University of Manchester, Manchester, M13 9PL, UK
[3] CCLRC Daresbury Laboratory, Warrington, Cheshire, WA4 4AD, UK

E-mail: eddie.snell@msfc.nasa.gov. and john.helliwell@manchester.ac.uk.

Abstract

Density difference fluid flows and sedimentation of growing crystals are greatly reduced when crystallization takes place in a reduced gravity environment. In the case of macromolecular crystallography a crystal of a biological macromolecule is used for diffraction experiments (x-ray or neutron) so as to determine the three-dimensional structure of the macromolecule. The better the internal order of the crystal then the greater the molecular structure detail that can be extracted. It is this structural information that enables an understanding of how the molecule functions. This knowledge is changing the biological and chemical sciences, with major potential in understanding disease pathologies.

   In this review, we examine the use of microgravity as an environment to grow macromolecular crystals. We describe the crystallization procedures used on the ground, how the resulting crystals are studied and the knowledge obtained from those crystals. We address the features desired in an ordered crystal and the techniques used to evaluate those features in detail. We then introduce the microgravity environment, the techniques to access that environment and the theory and evidence behind the use of microgravity for crystallization experiments. We describe how ground-based laboratory techniques have been adapted to microgravity flights and look at some of the methods used to analyse the resulting data. Several case studies illustrate the physical crystal quality improvements and the macromolecular structural advances. Finally, limitations and alternatives to microgravity and future directions for this research are covered.

   Macromolecular structural crystallography in general is a remarkable field where physics, biology, chemistry and mathematics meet to enable insight to the fundamentals of life. As the reader will see, there is a great deal of physics involved when the microgravity environment is applied to crystallization, some of it known, and undoubtedly much yet to discover.

Contents

1. Introduction

The key concepts that attracted crystal growers, macromolecular or solid state, to microgravity research are that density difference fluid flows and sedimentation of the growing crystals are greatly reduced. Thus, defects and flaws in the crystals can be reduced, even eliminated, and crystal volume can be increased.

Macromolecular crystallography differs from the field of crystalline semiconductors. For the latter, crystals are harnessed for their electrical behaviours. A crystal of a biological macromolecule is used instead for diffraction experiments (x-ray or neutron) to determine the three-dimensional structure of the macromolecule. The better the internal order of the crystal then the more molecular structure detail that can be extracted from the resulting diffraction data. It is this structural information that enables an understanding of how the molecule functions. This knowledge is changing the biological and chemical sciences, with major potential in understanding disease pathologies (Perutz 1992). Macromolecular structural crystallography in general is a remarkable field where physics, biology, chemistry and mathematics meet to enable insight to the fundamentals of life.

Growth of a macromolecular crystal in microgravity was first attempted on 20 April 1981 using Germany's Technologische Experimente unter Schwerelosigkeit (TEXUS 3) sounding rocket. A cine camera with Schlieren optics monitored the growth process of a crystal of the protein β-galactosidase. A laminar diffusion process was observed in contrast to turbulent convection seen in ground experiments (Littke and John 1984). The removal of this convection, the potential scientific and commercial payoff, and the fact that many experiments fit in a small volume gave rise to the general study and use of microgravity as a tool in macromolecular crystallization.

In this review, we examine the use of microgravity as an environment to grow macromolecular crystals. We describe the crystallization procedures used on the ground, how the resulting crystals are studied and the knowledge obtained from those crystals. We address the features desired in an ordered crystal and the techniques used to evaluate those features in detail. We then introduce the microgravity environment, the techniques to access that environment and the theory and evidence behind the use of microgravity for crystallization experiments. We describe how ground-based laboratory techniques have been adapted to microgravity flights and look at some of the methods used to analyse the resulting data. Several case studies illustrate the physical crystal quality improvements and the macromolecular structural advances. Finally, limitations and alternatives to microgravity and future directions for this research are covered.

1.1. Macromolecular crystallization in the laboratory

The aim of crystallization is to form a high quality crystal from the macromolecule of interest. In the case of biological macromolecules a crystal itself contains a significant solvent content, from 30% to 70% (Matthews 1968). Biological macromolecules are sensitive, stable only in relatively narrow temperature ranges and biochemical conditions. Crystallization involves many variables including the biological macromolecule itself, the buffer, the precipitant, the pH, the concentrations, the temperature etc. The macromolecules are large, e.g. a single polypeptide chain can consist of as many as 1000 amino acid residues, and can associate as 'oligomers' of individual macromolecule subunits in dimers, trimers, tetramers, etc. Any macromolecular subunit can have many degrees of freedom, i.e. highly flexible parts especially loops on the exterior of the macromolecule surface. Thus the crystallization process is complex and the field of crystallization has developed predominately
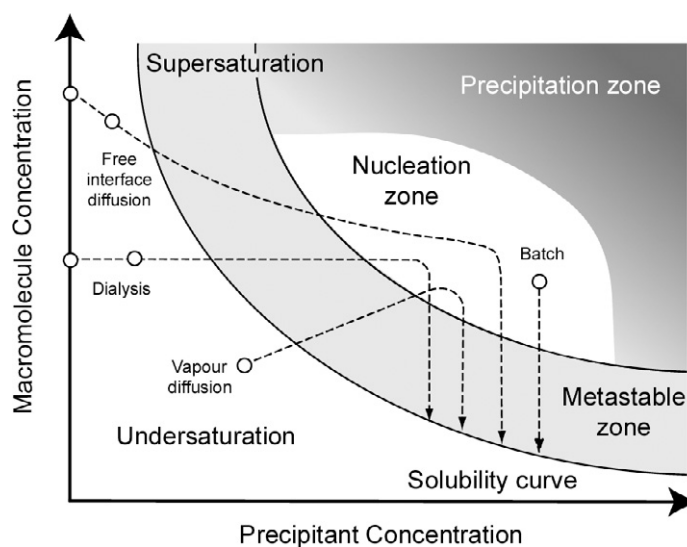
Figure 1. A schematic illustration of the macromolecular crystallization phase diagram based on two of the most commonly varied parameters, macromolecule and precipitant concentrations. The four main crystallization methods are highlighted showing that, in order to produce crystals, all the systems need to reach the same destination, the nucleation zone. In the case of dialysis and free interface diffusion (also called liquid/liquid diffusion) two alternative starting points are shown since the undersaturated macromolecular solution can contain solely the macromolecule or alternatively, the macromolecule with a low concentration of the precipitating agent. Adapted from Chayen (1998) with the permission of the IUCr.

as an empirical science but with studies on some fundamental aspects being possible (Chayen 2004).

Crystallization is in essence a phase transition phenomenon. Figure 1 shows a simplified example of a crystallization phase diagram based on the macromolecule concentration and the precipitant concentration. There are several regions of interest: the precipitation zone where the macromolecule will form an amorphous precipitate; the nucleation zone where spontaneous nucleation will take place; the metastable zone where crystals are stable and can grow but no further nucleation occurs; and the undersaturated zone where the macromolecule is fully dissolved in solution and does not crystallize. The metastable zone is thought to provide the best conditions for the growth of large well-ordered crystals.

There are several methods of crystallization, e.g. vapour diffusion, free interface diffusion, dialysis and batch (illustrated in figure 1), and temperature controlled crystallization. Vapour diffusion is widely used because it was the first to work with small quantities of sample thereby enabling screening for optimal conditions. In vapour diffusion, a droplet containing the macromolecule and a precipitant reservoir linked by a vapour pathway are set up in a closed chamber. As vapour transfer takes place, solution is lost from the drop containing the macromolecule and the concentration of both precipitant and macromolecule in solution increases. Using figure 1 as an example if the conditions enter the nucleation zone, nucleation occurs and hopefully, crystals start to form. At this point, the precipitant concentration in the crystallization drop is in equilibrium with that in the reservoir. As crystals grow the macromolecule concentration in solution is reduced and the conditions enter the metastable zone. Crystals continue to grow until the solution is undersaturated.

The free interface and dialysis methods are similar. The free interface diffusion growth technique consists of a macromolecule and precipitant solution diffusing into each other.

Both the total macromolecule and precipitant concentration are decreased from their initial values as each solution is effectively diluted by the other. There is a slow progression through the metastable state until equilibrium is reached. As the conditions enter the nucleation zone crystals nucleate and then grow in the metastable zone. As the macromolecule concentration in solution decreases, the solution becomes undersaturated and crystal growth ceases. In the dialysis method the macromolecule solution is behind a dialysis membrane as precipitant diffuses into it. Consequently, the macromolecule's concentration in solution remains constant until the experiment reaches the nucleation zone and then the macromolecule's concentration in solution decreases as crystals start to grow.

The batch method of crystallization is the oldest and simplest method. The precipitating agent is immediately mixed with the macromolecule solution bringing the solution to a state of high supersaturation. Under these conditions if crystals nucleate, the macromolecule's concentration in solution is reduced so the system enters the metastable zone where the crystals grow until the system reaches undersaturation.

Temperature controlled growth makes use of the variation of solubility with temperature for some macromolecules. The temperature is set at a point where the macromolecule is soluble then slowly changed until the macromolecule solubility is decreased and nucleation starts. As the temperature is further changed, the crystals grow until the solution is undersaturated.

A fundamental understanding of the biophysical chemistry of crystal growth exists. However, due to the complex nature of the system and the *a priori* unknown three-dimensional structure being crystallized, it is not yet possible to predict crystallization conditions from an amino acid sequence. There are a number of extensive empirical and theoretical texts on the subject (Bergfors 1999, Ducruix and Giege 1999, McPherson 1999, Chernov and Chernov 2002).

1.2. The science of structural crystallography

The study of a macromolecule with a light microscope is not possible as the scale of macromolecules is below the wavelength of visible light. Hard x-rays and neutrons (~ 1 Å) are of the correct wavelength to allow visualization in principle but cannot be focused by any known lens. Therefore, diffraction techniques are used and the image computed by Fourier analysis.

1.2.1. Macromolecular crystals, their symmetries and the basics of diffraction.

The diffraction of x-rays (or neutrons) from a macromolecular crystal allows the measurement of the intensities of reflections from which the macromolecular structure can be determined. The condition for constructive interference of the incident x-ray (or neutron) beam to produce a diffracted beam is governed by a grating equation $n\lambda = 2d \sin\theta$; this was first given for crystal diffraction in 1913 by Bragg who referred to diffraction orders from the crystal grating as reflections. Thus different orders of reflection, n, from families of atomic planes in a crystal (each described by the Miller indices (h, k, l) and interplanar spacing d) are stimulated at given diffraction angles θ, where 2θ is the angle between the incident and given diffracted beam. The theoretical limit of the d/n spacing is at $\theta = 90°$, i.e. $\lambda/2$. If the crystal is illuminated by a polychromatic beam of a band of wavelengths $\lambda_{min} < \lambda < \lambda_{max}$ then the crystal, held stationary, picks out the wavelengths that satisfy the Bragg equation possible reflections; this is called 'Laue geometry'. If a monochromatic x-ray beam is used then the crystal must be rotated continuously for Bragg reflections to occur. In Laue geometry any one exposure is equivalent to a certain rotation range of monochromatic geometry according to the wavelength bandpass (Helliwell 1992).

The total range of rotation coverage of a crystal needed to completely measure all the (h, k, l) Bragg reflection intensities does not need to be 360°. A crystal can possess internal symmetry. In general, there are 7 crystal systems, 14 ways of having centring (or no centring!) and finally 230 groups of symmetry elements that are possible, known as the crystal space groups. Biological macromolecules are handed molecules and thus some symmetry elements, mirror planes and inversion centres, do not occur. Thus biological macromolecules are found in only 65 of the 230 space groups. Cubic crystals are the most symmetric and just a few degrees of rotation of such a crystal are enough to capture the unique reflection data. Triclinic is the least symmetric and at least 180° of rotation is needed to stimulate all the unique reflection intensities.

1.2.2. Fourier analysis in crystallography. Each atom makes a different contribution to a reflection intensity according to its scattering strength for x-rays (or neutrons), its position and its mobility or relative disorder. By measuring a sufficient number of unique reflection intensities it is feasible to produce a refined molecular structure of defined precision. The mathematical relationships known as the structure factor equation (1.1) and the electron density equation (1.2) form a Fourier pair of equations between the 'diffraction space' and the 'real space' of the crystal atomic arrangement.

$$F(h, k, l) = \sum_{j=1}^{\text{atoms}} f(j) e^{[2\pi i (hx_j + ky_j + lz_j)]} \tag{1.1}$$

and

$$\rho(x, y, z) = \frac{1}{V} \sum_h \sum_k \sum_l F_{(hkl)} e^{[-2\pi i (hx + ky + lz)]}, \tag{1.2}$$

where $F_{(h,k,l)}$ is the structure factor for a particular set of planes defined by h, k and l, summed over all atoms in the basic repeating unit, $f(j)$, the atomic scattering factor of the jth atom with the coordinates (x_j, y_j, z_j). The unit cell volume is denoted by V and the electron density by ρ. The quantity $2\pi(hx_j + ky_j + lz_j)$ is the phase angle of the jth atom contribution to the overall structure factor. Equation (1.2) provides a means for calculating the electron density from the x-ray diffraction.

However, while the intensities of the diffraction spots (leading to Fs) can be measured the overall phase of each structure factor (i.e. each described by both amplitude and phase) cannot. This is termed the phase problem in crystallography and is well covered, along with crystallography methods in general, in various textbooks (Drenth 1999, Rossmann and Arnold 2001, Blow 2002, Giacovazzo 2002). In biological crystallography, the use of tunable synchrotron radiation to exploit the anomalous dispersion of the elements (i.e. the wavelength dependence of their x-ray scattering) has had a dramatic impact on solving the phase problem (Helliwell 1992).

1.2.3. The use of neutron beams. In the case of neutrons the quantity computed is the nuclear density since a neutron beam interacts strongly with the nuclei not with the atomic electrons. Neutron atomic scattering factors, unlike x-rays, are not monotonically increasing across the periodic table and, for some elements, e.g. hydrogen and manganese are negative, i.e. opposite in phase to other elements. Deuterium also scatters neutrons as strongly as carbon, nitrogen and oxygen. In practice a crystal structure is solved using x-rays, excluding the hydrogen atoms which are usually too weak to be seen or often cannot be put in calculated positions, and then the ordered isotopes of hydrogen are determined in full using neutron crystallography. Neutron

diffraction is especially useful for studying hydrogen atom positions or protonation states, key parameters in many biological functions that are often not revealed with x-ray studies. Neutron beams are weaker in magnitude than synchrotron x-ray beams, long measuring times are needed and crystals have to be large, i.e. $\sim 1\,\text{mm}^3$ or more for macromolecules of typical molecular weights ($\sim 30\,000\,\text{Da}$). Important breakthroughs in this field in recent years have included large area image plate detectors, use of longer wavelengths to enhance the scattering efficiency of the crystal and use of Laue geometry to maximize the number of neutrons utilized from the source, e.g. see Blakeley *et al* (2004a).

1.3. Diffraction from the crystal

1.3.1. Principles.   A good crystal enables the structure of the macromolecule to be solved to a resolution allowing useful information to be extracted. The total energy in a diffracted beam from a particular reflecting plane (h, k, l) for an ideally mosaic crystal rotating with a constant angular velocity ω through the reflecting position bathed in a monochromatic x-ray beam is:

$$E(h, k, l) = \frac{e^4}{m^2 c^4 \omega} I_0 \lambda^3 L P A \frac{V_x}{V_0^2} |F(h, k, l)|^2, \tag{1.3}$$

where I_0 is the intensity of the incident x-ray beam of wavelength λ, P is a correction for polarization, L is the Lorentz factor (a correction for the different velocities of the reciprocal lattice as it passes through the reflecting position; n.b. the reciprocal lattice is described in Buerger (1980) and many other crystallography textbooks), A is an absorption correction, V_x is the volume of the crystal and V_0 is the volume of the unit cell. For each reflection P, L and A as well as the structure factor amplitude $F(h, k, l)$ are different. In any single experiment, given a constant angular rotation, a constant incident intensity, a single fixed wavelength is used, the crystal is fully bathed in the x-ray beam and the unit cell is fixed, then several factors can be regarded as constants of proportionality for all the reflections, namely:

$$\frac{e^4}{m^2 c^4 \omega} I_0 \lambda^3 \frac{V_x}{V_0^2}. \tag{1.4}$$

Equation (1.3) strictly applies only to an ideally mosaic crystal or a crystal which scatters weakly. It is referred to as the kinematic diffraction approximation. The point of this idealization is that it avoids treating interference effects from the scattered beams with the incident beam. Such secondary effects are important with perfect, strongly scattering crystals and hence require a 'dynamical theory of diffraction'. For a description of perfect crystals and their diffraction properties see Authier (2003). Perfect crystals of silicon or germanium are well known cases where dynamical theory must be applied. For protein crystals, even if perfect crystals might be produced, they will remain in the kinematical approximation for all except the very strongest reflections, due to the generally weak scattering of macromolecular crystals. Theoretical considerations of the idealized limit of a perfect macromolecular crystal and its properties were first discussed by Helliwell (1988).

The sum over the reflections, equation (1.2), labelled by the Miller indices (h, k, l), is over all the measurable reflections but inevitably is up to a certain limit where the reflection intensity becomes too weak to be visible to the measuring apparatus. Situations also occur where the apparatus itself has an insufficient geometric aperture to measure all the available reflections. Either way this limit is called the resolution limit, '$d_{\min}$', of the data. The number of measurable reflections up to this limit is inversely proportional to $d_{\min}^3$. The more diffraction data (reflections) one has, the more precise will be the refined macromolecular structural model.

Given this, it makes sense to minimize factors contributing to the weakening of the diffracted signal at increasing resolutions so that as many reflections as possible can be measured.

The factors contributing to the weakening of the diffraction signals include:

(1) the fall off of x-ray atomic scattering factors with diffraction angle (n.b. not so with neutrons due to the relatively small nucleus being the scattering centre compared to the larger electron charge cloud for x-rays),
(2) thermal motion of the atoms accentuating their individual scattering factor fall off,
(3) the sample may not tolerate prolonged exposure (i.e. radiation damage occurs; true for x-rays but not a problem with neutrons which do not cause reactive, damaging, 'free' electron radicals in the sample),
(4) partial or full disorder of the atoms: the external, more mobile, loops of a macromolecule being a particular category of such cases,
(5) the crystal may have a very high solvent content (even as high as 85%) which also allows the ordered macromolecules to be more mobile than if held in a tightly packed crystal lattice,
(6) the source of radiation may be weak and similarly the sample may be small, and the unit cell volume large, thus having a weak scattering efficiency (equation (1.3)),
(7) the crystal may be mosaic so that the sharpness of the diffraction piling up at one specific diffraction angle for that reflection is not so well obeyed.

Another effect that results in an apparently weakened diffraction signal is the background noise. Contributions to this background are:

(1) marked diffuse scattering in the diffraction pattern arising from the solvent in the crystal and any disordered parts of the macromolecule (for a range of examples see Glover *et al* (1991)),
(2) air scatter as the primary beam passes en route to the detector via the sample (the reflections themselves also contribute air scatter but individually at a reduced amount),
(3) the crystal mount (a glass capillary in room temperature data collection or a nylon loop in cryo data collection),
(4) Compton scatter; this increases if very short x-ray wavelengths are used,
(5) detector noise.

Some of these factors are physical properties and cannot be minimized. Others, e.g. thermal motion of the atoms and overall crystal sample radiation damage can be reduced using cryocooling techniques (Garman and Schneider 1997, Garman 1999). Partial or full molecular disorder might be improved by co-crystallization of the macromolecule with a ligand ('fastening down' inherent flexibilities in the structure) or finding conditions that result in a new space group with more ordered packing. Similarly, solvent content may be reduced by packing efficiency in a different space group. Air scatter can be reduced by using helium beam paths in the diffraction 'camera'. Detector noise can be reduced by improved detector design. As we will explain, microgravity crystal growth has been used to help in three of these areas, namely reducing molecular diffuse scatter (probably via increasing short-range, intermolecular order), and increasing long-range order by both increasing the crystal volume and reducing the crystal mosaicity.

1.3.2. Diffuse scattering from the crystal. The use of microgravity crystal growth to reduce diffuse scattering has already borne fruit in small molecule studies (Ahari *et al* 1997). What is diffuse scattering? Basically, not all the diffracted photons from crystals end up in the Bragg reflections from specified (h, k, l) planes. Indeed, and it is true for quite a large number of

macromolecular crystals, the non-Bragg diffraction or diffuse scattering is strong in intensity. The diffuse scattering is due to a breakdown in the periodicity of the crystal and carries information on the mobility and flexibility of the molecules in the crystal (Welberry 2004). It may arise from several sources including:

- thermal diffuse scattering,
- static disorder scattering,
- solvent disorder.

The static or dynamic displacement of atoms in crystals causes a breakdown of translational symmetry of the crystal, leading to a reduction in the Bragg intensities at high resolution and the appearance of diffuse scattering at and between the reciprocal lattice positions. In the case of macromolecular crystals, diffuse scattering is often quite strong, can be rich in detail and apparently distinctive to a specific macromolecule and/or crystal. It represents a potentially valuable source of information regarding atomic displacements. Static disorder arises when unit cells exist with different arrangements of the time-averaged positions. Static orientational disorder occurs in molecular crystals where molecules, flexible domains, or side groups take up different orientations breaking the translational symmetry.

Dynamic disorder arises from thermal vibrations and is present in all crystals. Two types of lattice vibrations may be distinguished, acoustic modes due to the propagation of ultrasonic waves in the crystal and optic modes of vibration such as are observed in infrared and Raman spectra. Ultrasonic vibrations give rise to thermal diffuse scattering, which peaks primarily at the reciprocal lattice positions and is observed characteristically as a feature at and around the Bragg peaks. Optic mode vibrations along with other disorder modes give rise to diffuse scattering, which is distributed continuously but non-uniformly throughout reciprocal space.

1.3.3. Short-range order. Good short-range order in a crystal is a primary driver yielding high-resolution diffraction. An atom will contribute coherently to the intensity of a reflection only if its disorder relative to symmetry-related atoms is small. Figure 2 dissects the various disorders that can occur on the molecular scale within a crystal. First, atoms can be displaced by thermal vibrations; second, they can have multiple or partial occupancies; third, their position may be uncertain, especially in the case of waters and fourth, there may be variations in the main chain or side chains and in the inter-molecular packing. Diffusion limited, convection free, growth in a reduced acceleration environment is not likely to improve most of these short-range order perturbations since Brownian motion is a strong effect at this length scale. However, one aspect that it may be expected to help with, i.e. on this short length scale, is in improving intermolecular packing. By removing the turbulent buoyancy-driven convection of the crystal growth solution the attachment of macromolecules to the growing crystal becomes a sedate process limited by diffusion rather than kinetic considerations.

Short-range order can also be measured by the temperature factor, the so-called B factor. An overall B factor for the crystal can be calculated from a Wilson plot (Wilson 1942) where E_{obs} is plotted against $(\sin\theta/\lambda)^2$. The B factor is extracted from the slope of this plot $(-2B)$ as:

$$E_{\mathrm{obs}}(h, k, l) = E_{(h,k,l)}e^{(-2B\sin^2\theta/\lambda^2)}, \tag{1.5}$$

where $E_{\mathrm{obs}}(h, k, l)$ is the observed intensity of a reflection (energy from the diffracted beam), $E_{(h,k,l)}$ is the intensity if the atom were at rest, and B is the temperature factor. The Wilson plot also provides a scale factor, where it crosses the vertical axis, allowing intensities to be put on an absolute scale.

For a macromolecule there is considerable shape to this plot and a curve rather than a straight line is seen at resolutions around 4 to 3 Å. This is due to the nature of macromolecular
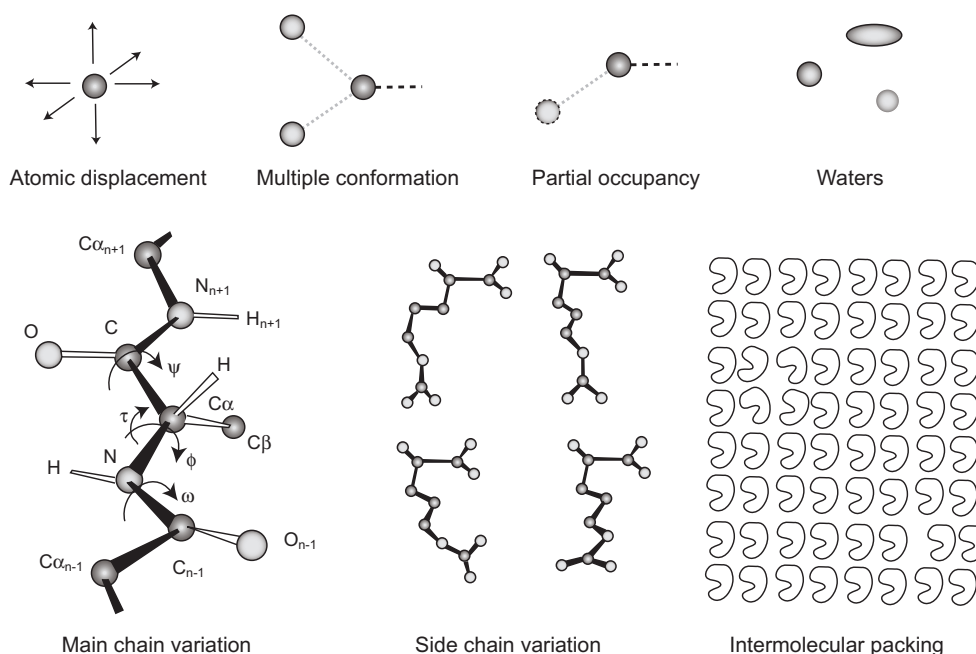
Figure 2. Contributors to the reduction of short-range order within a macromolecular crystal.

sub-structures (known as secondary structures, especially alpha helix and/or beta sheet (Eisenberg 2003)), and their regular hydrogen bonding distances, and causes the molecular transform to peak at these (reciprocal) distances. At higher resolution this results in a straight line and an accurate assessment of the B value becomes possible. The weakness of this parameter as the sole judge of optimal crystal growth conditions is that it is only an average indicator of the innate flexibilities of the protein.

1.3.4. Long-range order. Long-range order is a whole-crystal length-scale effect. Good long-range order results in high signal-to-noise in the reflection profiles, a small mosaicity and larger crystals. Figure 3 illustrates how long-range disorder contributes to broadening the resulting diffraction reflection profile. The mosaic model of crystals was proposed by Darwin (1922) and approximates the crystal to an array of perfectly ordered volumes (domains) slightly misaligned with respect to each other (the boundaries between these domains are ignored and no model for them is proposed). In addition to having small random misalignments, the domains can be of varying volume and the unit cells in the crystal can vary. Each of these phenomena has a distinct effect on the crystal (Nave 1998, Boggon *et al* 2000). In the case shown in figure 3(*a*) all the domains are well aligned so their contributions to the reflection overlap. Misalignment of the domains broadens the reflection profile reducing the signal-to-noise. If the volume of the domains becomes small, the reflections will become broadened from Fourier truncation effects (the transition from diffraction grating to a few slits is the analogous situation in optical diffraction and interference theory). The effect is known as domain-size broadening. A lattice parameter variation, figure 3(*c*) causes a reflection to have a range of slightly different Bragg angles also resulting in a smearing out of the reflection.

Long-range disorder in the crystal gives rise to localized effects in reciprocal space (Nave 1998, Boggon *et al* 2000). Improved long-range order in a crystal reduces the mosaicity and
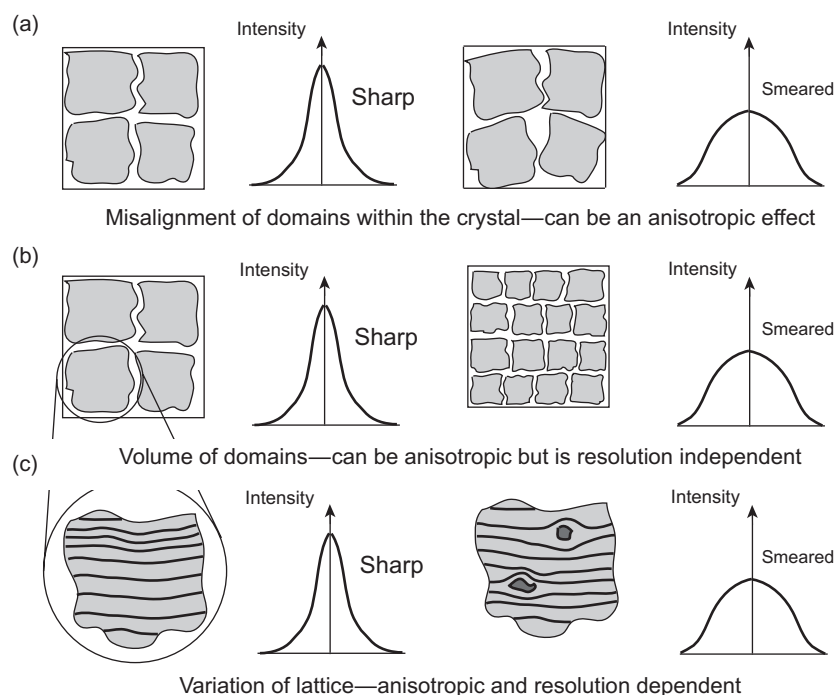
Figure 3. Long-range disorder and the resulting effect on the diffraction profile.

results in an increase in the resulting signal-to-noise of the reflections. One can readily imagine how the reduction of convection and sedimentation in the fluid during microgravity crystal growth can be of benefit to the stability of conditions for nucleation and for growth to a fully-fledged crystal.

1.3.5. Crystal volume. The final requirement of a good crystal is that it is of sufficient volume to produce measurable diffraction. In the extreme case for x-ray diffraction using a specialized microfocus synchrotron beamline, structural information can currently be extracted from crystals as small as 20 μm in diameter (Hedman *et al* 1985, Pechkova and Nicolini 2004a, 2004b). For neutron diffraction the requirement is approximately 1 mm^3 or greater.

2. Why make use of microgravity to produce good crystals?

This revolves around the supplementary question—how can microgravity affect macromolecular crystal growth? We can immediately rule out microgravity directly affecting the internal flexibility of a macromolecule unless it is at the surface where it interacts with a neighbouring macromolecule in the lattice. We can look at the effect of microgravity on two levels, nucleation and subsequent crystal growth.

2.1. Nucleation

The initial process in macromolecular crystal growth, namely nucleation, involves solute–solvent/precipitant interactions. For microgravity to have a direct effect implies that it significantly affects the bond energies at the molecular level; *that gravitational forces at the*

molecular scale are comparable in magnitude to the intermolecular forces. If so, then other physical properties such as boiling and freezing points, enzyme kinetics, etc, would be affected as well. This has not been observed to date (Giachetti *et al* 1999).

Secondary nucleation is the formation of nuclei in solutions that already contain growing crystals. In a $1g$ field and a crystal of size $\sim$10–100 μm, buoyancy-driven flows develop which not only maintain a high growth rate, but may also produce increased secondary nucleation (Pusey and Naumann 1986, Pusey *et al* 1988, Grant and Saville 1995). Secondary nucleation is thought to be caused by the removal of partially solvated clusters from near the surface of the crystal (the absorbed layer) by this flow (Larson 1991). Reduced buoyancy-driven flows in microgravity reduce this effect.

2.2. Growth

The standard model for understanding the effects of microgravity on macromolecular crystal growth is based on the concept of a depletion zone (McPherson *et al* 1991). In the absence of acceleration, a crystal is subject to Brownian motion as on the ground, but unlike the ground case, there is no acceleration inducing it to sediment. A growing crystal in zero gravity will not move with respect to the surrounding fluid. Moreover, as macromolecules leave solution and add to the crystal, a region of solution depleted in protein is formed. Usually this solution has a lower density than the bulk solution and will rise upward in a $1g$ field as seen in both small molecule (Chen *et al* 1979) and macromolecular crystallization (figure 4) (Pusey *et al* 1988). In zero gravity, the buoyancy force is eliminated and no buoyancy-driven convection occurs.

Because the position of the crystal and its depletion zone are stable in microgravity, the crystal can grow under conditions where its growing surface is in contact with a solution that is slightly supersaturated. In contrast, the sedimentation and convection that occur under $1g$ place the growing crystal surface in contact with bulk solution that is typically several times supersaturated. Lower supersaturation at the growing crystal surface allows more high-energy mis-incorporated growth units to disassociate from the crystal before becoming ideally oriented and trapped in the crystal by the addition of other growth units. However, since microgravity is not in fact zero gravity (see section 3), the buoyancy-driven convection and sedimentation are only attenuated rather than eliminated. Promotion of a stable depletion zone in microgravity is postulated to provide a better ordered crystal lattice and benefit the crystal growth process.

Model calculations and limited empirical data suggest that accelerations greater than $1\mu g$ will perturb macromolecular crystallization. A summary of flow effects on macromolecular crystal growth in microgravity is presented in section 4. A more empirical treatment is described elsewhere (Boggon *et al* 1998, Helliwell *et al* 2002).

3. The microgravity environment

Microgravity is not an accurate term to describe the environment experienced on an orbiting spacecraft. The reduced acceleration is achieved through free fall as the spacecraft orbits the Earth. The term microgravity is used both in colloquial and scientific senses. In the colloquial sense it means an acceleration level much less than unit gravity, $g = 9.8\,\mathrm{m\,s^{-2}}$. In the strict scientific sense microgravity means on the order of $10^{-6}g$, i.e. μg. We will use it in the colloquial sense since true, constant $10^{-6}g$ is not realized in practice.
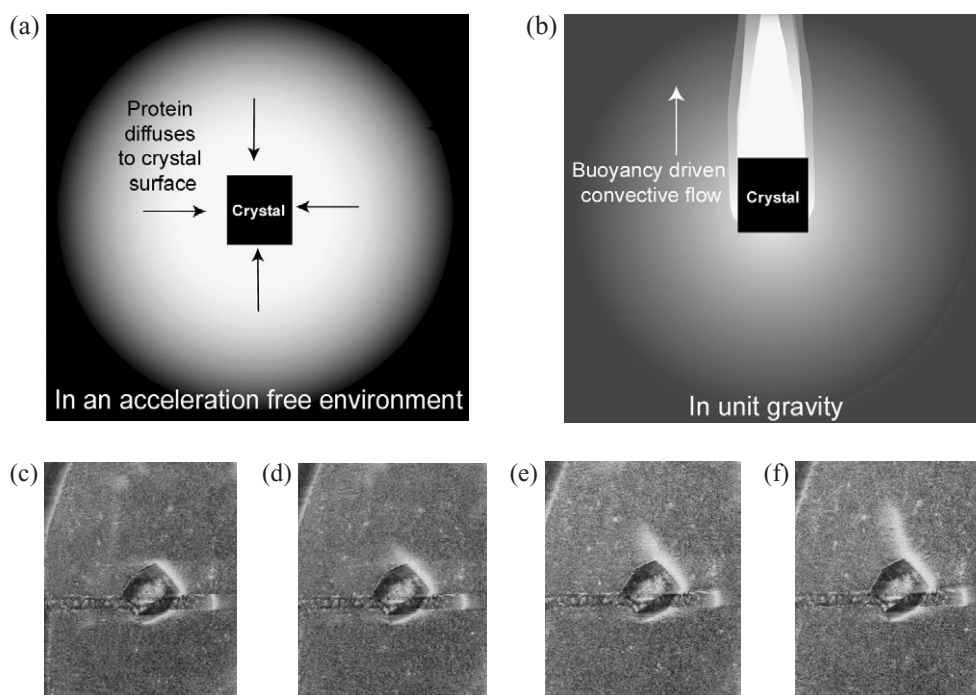
Figure 4. Illustration of the zone of depleted macromolecule around a growing crystal in (*a*) schematic of an acceleration free environment compared to the convective plume formed by growth in (*b*) unit gravity. Also shown (*c*)–(*f*) are Schlieren photography images of the convective plume that forms over time from a lysozyme crystal (approximately 1.2 mm in size) grown on the ground (Pusey *et al* 1988), the time interval between each image is 12 s giving a plume velocity of approximately 30 μm s^{-1}.

3.1. How is microgravity achieved?

Newton's law of gravitation states that the force, F, between two masses, M and m, at a distance r apart is proportional to the product of the masses and inversely proportional to the square of the distance between them, i.e. an object at height h above the surface of the Earth, assuming a spherically symmetrical mass distribution, experiences a force given by

$$F = G\frac{M_e m}{(R_e + h)^2},\tag{3.1}$$

where G is the gravitational constant, m the mass of the object, M_e is the mass of the Earth and R_e its radius. If the object is dropped it will fall, i.e. accelerate towards the centre of the Earth with an acceleration, a, given by

$$F = ma,\tag{3.2}$$

$$a = \left(\frac{GM_e}{(R_e + h)^2}\right) = g.\tag{3.3}$$

This acceleration due to gravity is termed g.

In a typical low Earth orbit a spacecraft has an altitude on the order of $\sim$400 km. The Earth has a radius of approximately 6.4×10^6 m hence the acceleration due to gravity that an object experiences onboard the spacecraft is approximately 90% of that experienced on the

Earth. True microgravity, considering the Earth alone, is then experienced only at a distance of about 6×10^9 km from the Earth (about 40 times the Earth–Sun distance)!

The microgravity environment experienced by low Earth orbit spacecraft is not produced from sending the spacecraft away from the Earth into space but from the fact that, while orbiting the Earth, the spacecraft is in free fall. As the spacecraft is moving with a constant velocity v in a circular orbit, the velocity is always varying because the direction of v is changing. This changing velocity is acceleration towards the centre of the circle with magnitude v^2/r where r is the radius of the orbit. The velocity that a spacecraft in a circular orbit must have in order to achieve an acceleration g towards the centre of the Earth (and hence zero acceleration at its centre of mass) is given by

$$v = \left(\frac{GM_e}{R_e + h} \right)^{1/2}. \tag{3.4}$$

For an orbit at 400 km from the Earth's surface the spacecraft's velocity has to be 7.7 km s^{-1}. Only the centre of mass of the spacecraft will have acceleration equal to g. For every 1 m away from the centre of mass an object experiences a $10^{-7}g$ force to constrain it to a fixed position relative to the centre of mass.

Any object in free fall towards the centre of the Earth experiences a reduced relative gravitational acceleration. Orbital spacecraft allow that free fall to last for the duration that the spacecraft remains in orbit, i.e. days to weeks. Drop towers, where an experiment is dropped on Earth, give a reduced acceleration environment lasting on the order of seconds. Aircraft flying parabolic trajectories produce an acceleration of $10^{-2}g$ over 25 s with a period of 5–15 s of acceleration as low as $10^{-3}g$ during the pushover at the top of the parabola. Capsules dropping to Earth after being lifted by high altitude balloons offer $10^{-2}g$ to $10^{-5}g$ for $\sim$1 min. Sounding and suborbital rockets give longer periods (on the order of several minutes) at $10^{-5}g$ (Stavrinidis *et al* 1991).

3.2. What microgravity environment can be achieved?

A spacecraft is a single body in which any vibration is transmitted to the rest of the body, there being insufficient mass to damp it. Oscillatory accelerations also known as g-jitter arise from crew exercise and activity, the operation of experimental and life support equipment and harmonic structural vibrations of the spacecraft itself (Snell *et al* 1997a, Boggon *et al* 1998, Matsumoto and Yoda 1999). Accelerations experienced onboard an orbiting spacecraft can be characterized as quasi-steady, oscillatory or transient. Quasi-steady accelerations (frequency less than 0.01 Hz) result from atmospheric drag, venting of air or water and the 'gravity gradient' across the spacecraft. They are typically low magnitude (1μg or less). The amount of atmospheric drag depends on the attitude of the orbiting vehicle, i.e. a Space Shuttle Orbiter flying nose-first has less drag than an Orbiter flying belly first. The term gravity gradient refers to the forces that arise as different parts of the vehicle follow different orbital trajectories. Only those parts of the vehicle that lie on the orbital trajectory of the vehicle's centre of mass are free from inertial forces. The parts not on this trajectory experience a residual inertial force because their orbital trajectory is not the same as the centre of mass. A position above the centre of mass has a higher orbital radius and slower velocity relative to the centre of mass so an inertial force is required to keep it in the same position relative to the centre of mass. Gravity gradient forces produce accelerations of about 0.1–0.3μg per metre of displacement from the orbital trajectory of the centre of mass.

Figure 5 illustrates the typical acceleration environment in the form of a principal component spectral analysis (PCSA) (DeLombard *et al* 1997) for microgravity dedicated and
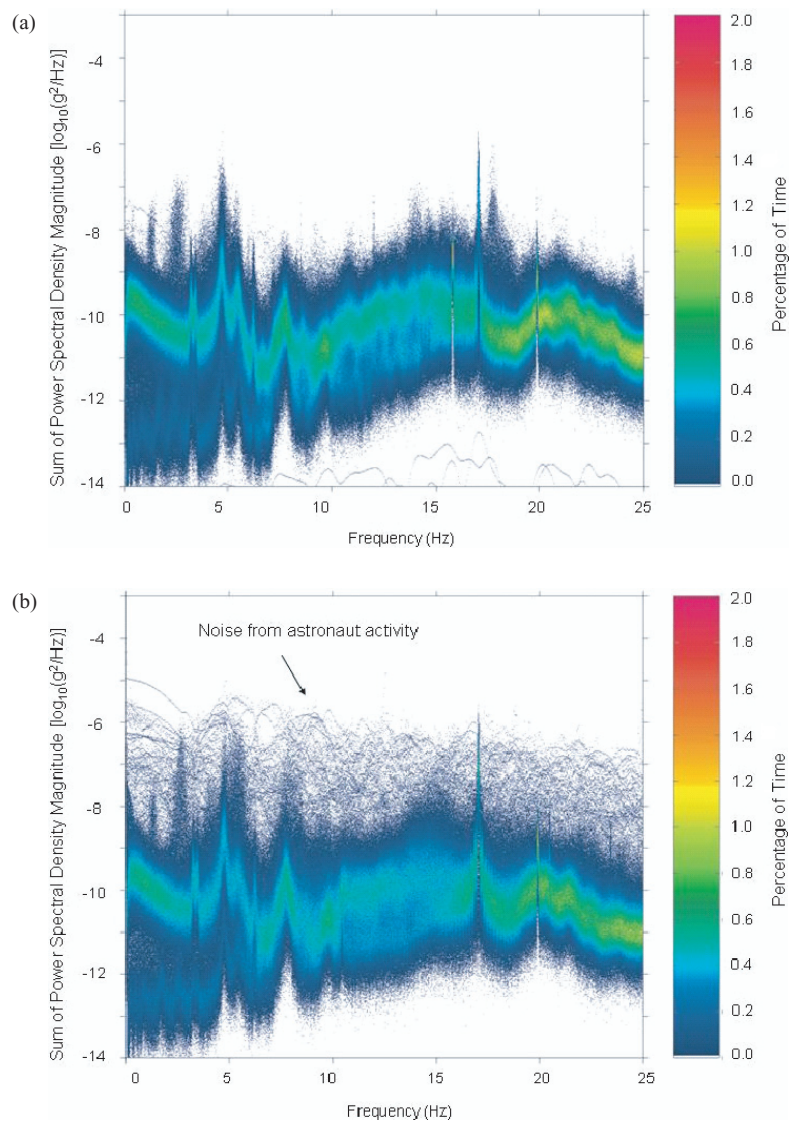
Figure 5. PCSA plots for the STS-62 mission showing (*a*) acceleration during rest time and (*b*) acceleration during the a time when the crew were awake and active.

non-microgravity dedicated parts of the same Space Shuttle mission, STS-62. The PCSA is a frequency-domain analysis technique that accumulates power spectral density magnitudes and frequency domains from accelerometers positioned throughout the Orbiter. The plots show magnitude, time (colour) and frequency. These data provide a snapshot of the acceleration environment during the mission. There is significantly more short duration acceleration noise in the non-dedicated microgravity time seen in the upper part of figure 5(*b*).

The microgravity environment on the International Space Station (ISS) has been measured (Jules *et al* 2004a, 2004b). Initial design requirements are that 50% of the International Standard Payload Racks (the Space Station equivalent of a laboratory bench) must have quasi-steady accelerations below $1\mu g$ for periods of at least 30 days six times a year. The vibration

environment is similarly specified as a function of acceptable accelerations for a frequency range from 0.01 to 300 Hz. The ISS is still a construction site so it is of no surprise that it does not yet meet its design requirements. For experiments that are sensitive to disturbances below 25 Hz and especially for experiments sensitive to disturbances below 5 Hz there is significant advantage to performing these during crew sleep time or when few activities are taking place (Jules *et al* 2004a, 2004b).

4. Theoretical studies on macromolecular crystal growth in microgravity

4.1. Background

The Navier–Stokes equations are the fundamental partial differentials that describe the flow of incompressible fluids. For a non-rotating frame,

$$\frac{\partial u}{\partial t} + u \cdot \nabla u = -\frac{\nabla P}{\rho} + v \nabla^2 u + \frac{F}{\rho}, \tag{4.1}$$

where u is the fluid velocity, P is the pressure, ρ is the mass density of the fluid, v is the kinematic viscosity of the fluid and F is the externally applied force per unit volume. The kinematic viscosity is defined in terms of the viscosity, μ, as $v = \mu/\rho$. The continuity equation expresses the conservation of mass in the system, that is,

$$\nabla \cdot u = 0. \tag{4.2}$$

In a crystallization experiment where crystal growth has started there are several species in solution that are transported to the growing crystal. Lin *et al* (1995) express the transport of momentum and species in solution in a dimensionless form using the Boussinesq approximation,

$$\frac{\partial U}{\partial t} + U \cdot \nabla U = -\nabla P + \nabla^2 U + \sum_j \frac{Ra_j}{Sc_j} \bar{\rho}_j g, \tag{4.3}$$

$$\frac{\partial \bar{\rho}_j}{\partial t} + U \cdot \nabla \bar{\rho}_j = \frac{1}{Sc_j} \nabla^2 \bar{\rho}_j, \tag{4.4}$$

where U, P and g are the dimensionless mass average velocity vector, pressure and gravitational acceleration vector, respectively. The dimensionless species mass density, $\bar{\rho}_j$ is defined as $(\rho_j - \rho_j^0)/\rho_j^0$, where ρ_j^0 is the initial uniform mass density of component j (macromolecule and precipitant) in the solution. The dimensionless Rayleigh and Schmidt numbers for component j are defined as $Ra_j = w^3 g_0 \beta_j \rho_j^0 / D_j v$ and $Sc_j = v/D_j$, respectively. Here w is the crystal width, g_0 is the terrestrial acceleration, D_j the component diffusivity, B_j the component solutal expansion coefficient and v the kinematic viscosity, $v = \mu/\rho$ where μ is the viscosity and ρ is the density of the fluid. The Rayleigh number is a product of the Grashof number (approximating the ratio of buoyancy force to viscous force acting on a fluid) and the Prandtl number (approximating the ratio of momentum diffusivity and thermal diffusivity). The Schmidt number describes the ratio of kinetic viscosity to molecular diffusivity.

The transport of a macromolecule to a crystal face under different acceleration conditions can be predicted from the fundamental fluid physics above (Lin *et al* 1995). To accurately model the crystal growth and hence the change in concentration around the crystal accurate knowledge about the crystal growth rate dependence on supersaturation is required. Fluid flow in microgravity is well described by Monti (2001).

4.2. Steady state residual acceleration effects

The effects of steady state residual acceleration have been modelled for the crystal growth of the enzyme lysozyme. Castagnolo *et al* (2001) numerically modelled the free interface diffusion technique using a cell of height 40 mm and length 10 mm. Under unit-gravity rising plumes of the enzyme developed at the boundary walls and centre of the interface. The central plume spread vertically with the two boundary plumes reaching the top and bottom walls some 900 s after the diffusion started. This caused further turbulence in the cell. At an acceleration of $10^{-6}g$ there is a smooth concentration gradient after 2 h with a maximum stream function of $10^{-7}\,\text{cm}^2\,\text{s}^{-1}$, i.e. convection is very slow. Castagnolo *et al* (2001), modelled only the solution diffusion and made no attempt to model the crystal growth. Lin *et al* (1995) modelled a growth cell of 1 mm height and 6 mm width containing a lysozyme crystal 0.6 mm wide and 0.4 mm high placed in the centre of the bottom cell wall. Using a finite element numerical model it was shown that a solution-convecting field evolves rapidly around the growing crystal in unit acceleration with the maximum solution velocity occuring near the upper corner of the crystal. Calculated enzyme concentration fields show strong convective transport contributions but in the absence of acceleration these are replaced with boundary layers of concentration around the growing crystal. This is called the depletion zone where growth becomes dominated by diffusion and the probability of parasitic nucleation is reduced. Figure 6(*a*), taken from data presented in Lin *et al* (1995), shows the normalized macromolecule concentration as a function of time and distance from the growing crystal face. On the ground, in unit acceleration, the concentration rapidly increases to a constant level away from the crystal face. In the absence of gravity, zero acceleration, the increase in concentration is far more subtle.

Ramachandran *et al* (1995) also used numerical modelling for a generic macromolecular crystal. The maximum velocity in the resulting flow field from the buoyancy-driven plume of the growing crystal was $455\,\mu\text{m}\,\text{s}^{-1}$ at $1g$ decreasing to $0.037\,\mu\text{m}\,\text{s}^{-1}$ in $10^{-5}g$. Similarly, the maximum velocity of the flow above the centre of the crystal is $90\,\mu\text{m}\,\text{s}^{-1}$ at $1g$ decreasing to $0.04\,\mu\text{m}\,\text{s}^{-1}$ in $10^{-5}g$. This is illustrated in figure 6(*b*) taken from data in Ramachandran *et al* (1995). The decrease in acceleration results in a rapid decrease in flow rate. Cang and Bi (2001) modelled liquid/liquid diffusion crystallization based on a flown experiment. They had a 20 mm high, 3 mm wide growth cell containing a 0.6×0.6 mm seed crystal at a point known from experiment to have the maximum probability of nucleation. In this case, the density of the lysozyme solution in the upper part of the cell was smaller than the precipitant salt solution. On the ground, after 1 s, flow rates reached $21\,\mu\text{m}\,\text{s}^{-1}$ in the top corner of the crystal slowing to $16.4\,\mu\text{m}\,\text{s}^{-1}$ after 1 h. Profiles of the lysozyme concentration display a very similar trend to those shown in figure 6(*a*).

Sedimentation of the growing crystals is reduced with a reduction in acceleration. The instantaneous distance travelled by a crystal in solution due to a residual acceleration can be approximated by

$$l = \frac{2}{9}\frac{R^2 g(\rho_\text{c} - \rho_\text{s})t}{\mu}, \tag{4.5}$$

where l is the distance moved in time t, μ is the solution viscosity, ρ_c is the crystal density and ρ_s the solution density, R is the crystal radius and g is the acceleration acting on the crystal. The relationship is approximate because it makes assumptions that the crystal has reached the Stokes settling velocity, crystal shape is approximated by a sphere, only a single averaged impulse is considered and, no allowance for crystal growth kinetics is made. In the case of lysozyme crystallization, Pusey and Naumann (1986) give $\rho_\text{c} = 1.45\,\text{g}\,\text{cm}^{-3}$, $\rho_\text{s} = 1.00\,\text{g}\,\text{cm}^{-3}$ and μ as $1.45 \times 10^{-2}\,\text{g}\,\text{cm}^{-1}\,\text{s}^{-1}$. Using these values the terminal sedimentation velocity
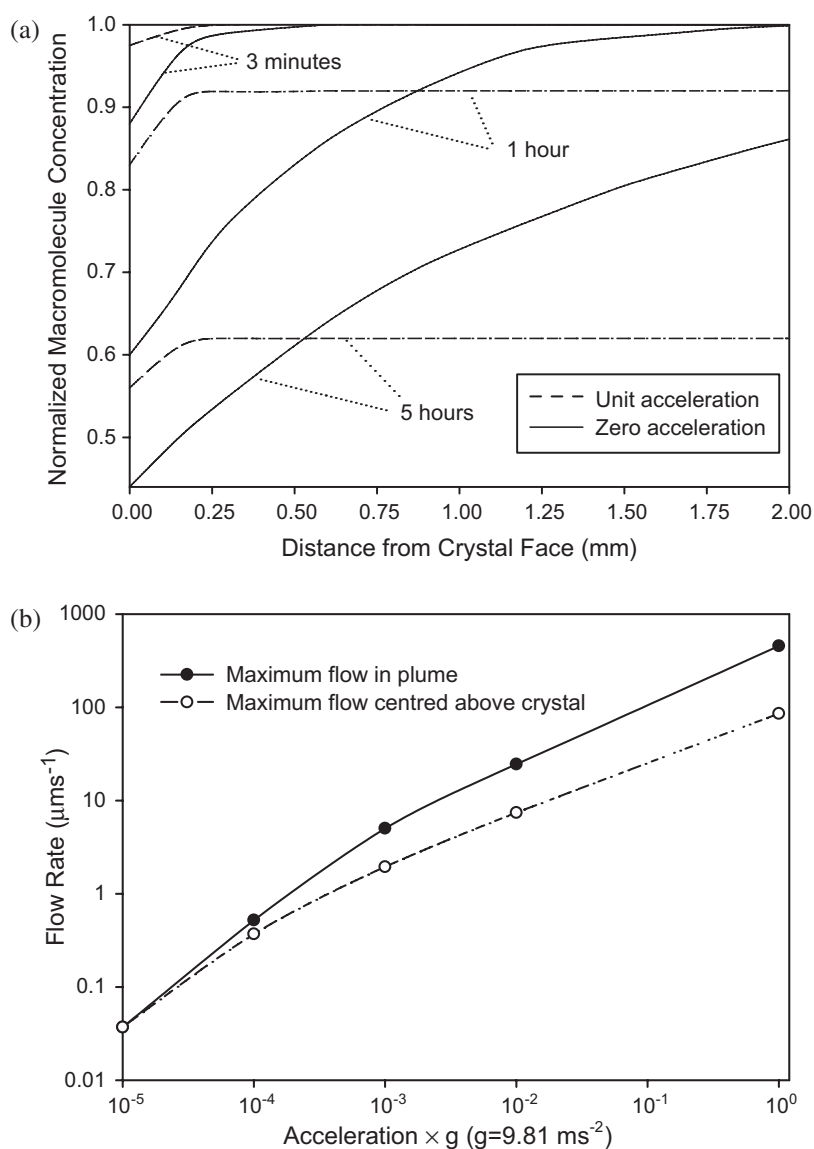
Figure 6. Plots illustrating the effect of steady state acceleration on growing crystals. From Lin *et al* (1995) (*a*) shows the normalized macromolecule concentration, in this case lysozyme, as a function of time and distance from the growing crystal face in unit acceleration and zero acceleration. The effect of acceleration level on flow rate is shown in (*b*) with data taken from Ramachandaran *et al* (Ramachandran *et al* 1995).

(Stokes settling velocity) of spherical crystals as a function of crystal radius and acceleration level can be estimated, figure 7.

For a small crystal, e.g. 10 μm grown at $10^{-5}g$, sedimentation would take just over 8 days (i.e. $8 \times 24 \times 3600\,\text{s} \times 0.001\,\mu\text{m s}^{-1} = 600\,\mu\text{m}$), compared to approximately 8 s on the ground. The reduction in sedimentation in microgravity is an important parameter that keeps the crystal in suspension surrounded by nutrient and allows larger volume crystals to grow.
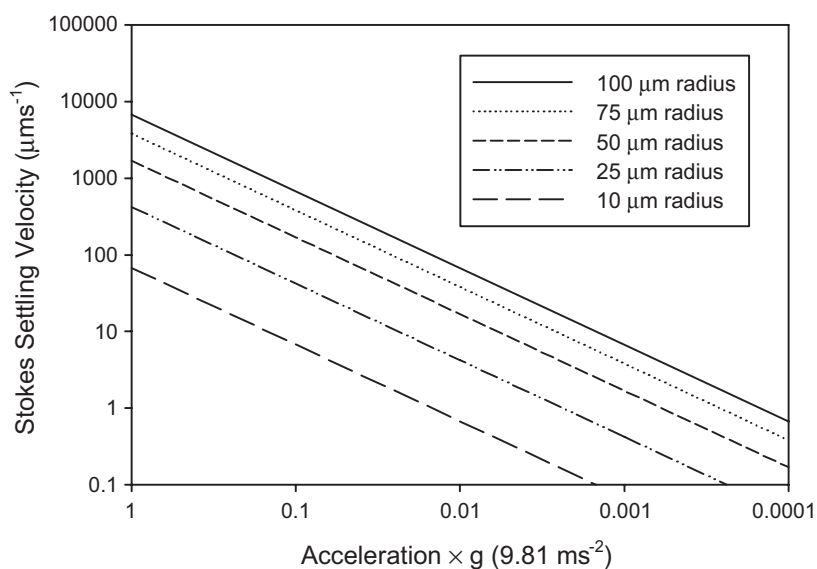
Figure 7. Stokes settling velocity for lysozyme crystals as a function of acceleration and crystal radius.

Qi *et al* (2000), numerically simulated both the sedimentation and buoyancy-driven convection as a crystal grew. They looked at lysozyme batch crystallization in a 5×5 mm cell with the cylindrical crystal (diameter equal to height) suspended in the centre of the cell when $\leqslant 10 \,\mu$m in diameter and a case with the crystal on the cell floor when $\geqslant 10 \,\mu$m in diameter. In unit gravity with a suspended crystal diameter of 1, 4 and $10 \,\mu$m the convection reached velocities of $1.4 \,\mu$m s^{-1}, $4.6 \,\mu$m s^{-1} and $7.7 \,\mu$m s^{-1}, respectively. For $1 \,\mu$m diameter crystals the concentration distribution for both unit and zero acceleration was very similar. As size increases buoyancy-driven flow is enhanced and slightly alters the purely diffusive conditions around the crystal seen under zero acceleration. In unit acceleration, as the crystal reaches a diameter above a few micrometres sedimentation flow starts to influence the convective flow. A new vortex is introduced which is opposite to the buoyancy-driven convective flow in the bulk solution and acts to reduce that flow. There exists a balance between buoyancy-driven convection and sedimentation until a critical size is reached. Under the case studied crystals started to sediment when they reached a minimum diameter between 3.5 and $4.6 \,\mu$m. When sedimented crystals with diameters of 10 and $100 \,\mu$m were considered growing at the bottom of the cell the plumes calculated had velocities of $9.8 \,\mu$m s^{-1} and $62.7 \,\mu$m s^{-1}, respectively. Local flow for the $10 \,\mu$m sedimented crystal case was smaller than that for a $10 \,\mu$m suspended crystal due to the restriction of the cell wall. The simulation showed that under normal gravity conditions the solution transport becomes dominated by buoyancy-driven convection when the crystal grows above several tens of micrometres.

Thus, each of the above studies demonstrates a theoretical foundation for the observations seen of an effect on the fluid and motion of crystals in microgravity.

4.3. Transient g-jitter effects

Vibrations or *g*-jitter can affect the growth of a crystal by causing the crystal to move around its environment and disrupt the idealized diffusion conditions. Similarly, sudden acceleration

can perturb, even temporarily destroy the depletion zones formed round the crystal and cause buoyancy-driven convection to result. Ramachandran *et al* (1995) modelled the effect of transient and periodic effects on crystals growing under microgravity. They considered a single, 1s duration, $10^{-2}g$ impulse, two 1 s duration, $10^{-3}g$ impulses in opposite directions separated by 1 s and a periodic sinusoidal $10^{-3}g$ acceleration. In the case of a single impulse, a flow field develops quickly with the most intense flow seen above the crystal. The concentration near the crystal face does not change until some minutes after the impulse but once established some minutes are needed to return to diffusion-controlled conditions. Significant perturbations to the concentration field are seen surrounding the crystal. The second impulse in the opposite direction resulted in much reduced flow than the single impulse. The smaller residual flow was governed by how much the first flow decayed by the time the second impulse was applied. Perturbations to the concentration field were seen surrounding the crystal but these were reduced compared to the single impulse. There was virtually no change in the concentration field surrounding the crystal for the oscillating acceleration applied. The effect on concentration field is inversely proportional to the frequency of the oscillation with low frequencies giving the velocity field time to respond to the impulse.

For macromolecules there is limited work studying the effect of the frequency of the transient g-jitter. However the aqueous solution temperature controlled growth of an inorganic, triglycine sulphate crystal has been numerically simulated (Nadarajah *et al* 1990). Simulated growth was carried out with steady background accelerations of $10^{-6}g$ and $10^{-5}g$ with impulsive and periodic disturbances of higher magnitude imposed at intermediate points. The crystal was 1.2 cm in width, 0.4 cm in height and was placed on a 4.8 cm high plinth the width of the crystal in a cell containing nutrient 10 cm tall by 10.8 cm wide. Slow flow was seen around the crystal during growth. The disturbances numerically modelled were a $10^{-3}g$ 1 s duration impulse, 10^{-1} Hz periodic disturbances at 10^{-4}, 10^{-3} and $10^{-2}g$, 10^{-2} Hz periodic disturbances at 10^{-3} and $10^{-4}g$ and 10^{-3} Hz periodic disturbances at 10^{-3} and $10^{-4}g$. The response of the system to the disturbances was minimal (10% or less growth rate variations) until a critical frequency of disturbance was reached. Although this study was not carried out with a macromolecule its findings can be qualitatively extrapolated to the macromolecular case. The disruption to the growth by a periodic disturbance is related to the magnitude of the disturbance and inversely related to the frequency, e.g. high frequency impulses have less impact than low frequency impulses. Similar results were obtained by Matsumoto and Yoda (1999) who looked at the diffusion coefficient as a function of sinusodial varying acceleration and Ellison *et al* (1995) who used mission acceleration data to model suspended particles in solution. A classic example illustrating the influence of transient acceleration is the case of astronaut exercises breaking down depletion zones while higher frequency disturbances seen in accelerometer data had no observable effect on the macromolecular crystal growth (Snell *et al* 1997a). The studies by Nadarajah *et al* (1990) and Ramachandran *et al* (1995) are in good agreement as they both predict that keeping the acceleration at $10^{-6}g$ will ensure that the transport regime remains diffusion dominated. These are important results establishing that microgravity conditions can keep the crystal growth regime diffusion dominated.

4.4. Marangoni effects

A reduction in acceleration reduces the density-driven convective flow in crystallization experiments however this does not rule out another type of convection; in the case of the vapour diffusion crystallization technique there is a surface tension Marangoni convection effect, see figure 8. As explained in the introduction, vapour transfer takes place across
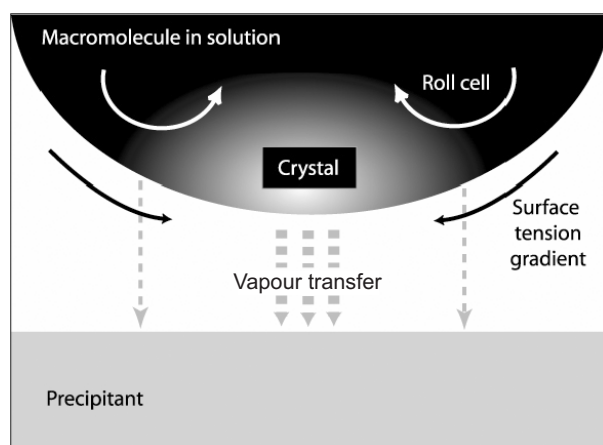
Figure 8. Schematic diagram showing a hanging drop in a zero acceleration environment to illustrate the causes of Marangoni convection. The roll cells illustrated describe the direction of fluid flow as the surface tension gradient equilibrates.

the boundary between the crystallization drop and the precipitant reservoir. Due to the geometry of the system the vapour transfer occurs at different rates over the drop surface and a surface tension and concentration gradient are established. Growing crystals are subjected to different concentrations on their faces and these concentration gradients lead to flow within the crystallization drop. Marangoni convection can occur on the ground depending on the solutions studied (Savino *et al* 2002) but is commonly masked by the more dominating buoyancy-driven convection in unit gravity (Kawaji *et al* 2003). The signature of cyclic motion of crystals under Marangoni convection conditions has indeed been observed during macromolecular crystal growth in microgravity (Chayen *et al* 1997).

4.5. Short-range effects?

Grant and Saville examined flow effects on macromolecular crystallization at the molecular scale (Grant and Saville 1991). Their analysis showed that shear forces are several orders of magnitude smaller than those required to break a single intermolecular bond. Those same forces were as much as eight orders of magnitude too small to strip macromolecules from the crystal surface. Flow around the crystal does not limit attachment although it has been observed to slow growth (Pusey *et al* 1988). Grant and Saville also considered the possibility of flow imparting a preferred orientation on the macromolecule. For lysozyme the rotational diffusion coefficient is $\sim 2 \times 10^7 \, \text{s}^{-1}$, i.e. randomization of the macromolecule occurs much faster than any fluid flow effects. Another possibility considered and rapidly dismissed was the denaturation of the macromolecules by the fluid flow. Grant and Saville (1991) found no evidence that buoyancy-driven convection mechanically alters the state of the macromolecule at or near the crystal face.

5. History of microgravity crystallization

There are a number of excellent reviews on the history and results of microgravity crystallization experiments (McPherson 1996, Kundrot *et al* 2001, Vergara *et al* 2003).

Here we provide a brief background covering the historical highlights and apparatus development. Some of the more commonly used apparatus is described in detail in section 6.

Littke conducted the first microgravity protein crystallization in April 1981 using Germany's TEXUS sounding rocket. The protein β-galactosidase was crystallized by liquid–liquid diffusion. In microgravity strictly laminar diffusion was observed, in contrast to turbulent convection on the ground. Several single crystals approximately $100 \, \mu$m in length grew in the 6 min of microgravity. These crystals were of inferior but of comparable visual quality to those grown on the ground (Littke and John 1984).

The USA NASA Space Shuttle programme had its first mission, STS-1 (STS standing for Space Transportation System), on April 12, 1981 with the first fully operational mission, STS-5, from November 11–16, 1982. The first Orbiter macromolecular crystal growth experiment was STS-9 (November 28–December 8, 1983). It was a joint NASA–European Space Agency (ESA) science mission carrying Spacelab. The apparatus was based on the TEXUS hardware design. The vapour diffusion method was used for the first time in microgravity on the STS-51D mission (April 12–19, 1985). Two vapour diffusion apparatus (VDA) were flown and many drops were lost during activation or deactivation. Iterative development and refinement of the VDA hardware took place on subsequent flights (DeLucas *et al* 1986).

The first unmanned extended duration, i.e. greater than 6 min, macromolecular crystallization experiments were carried out on the USSR Photon satellite mission, launched in April 1988. Trakhanov *et al* (1991) flew five proteins in a total of 21 liquid–liquid growth cells. A 30 S ribosomal subunit from *Thermous thermophilus* crystallized in microgravity but not on the ground, and catalase produced larger crystals in microgravity. However, experiments under optimal laboratory conditions, rather than ground control hardware, produced larger crystals. The other proteins did not produce crystals in microgravity or on the ground. In 1988, China launched China-23 carrying COSIMA-1 (Crystallization of Organic Substances in Microgravity for Applied Research). The apparatus consisted of a flexible tube containing protein and salt solution separated by an air gap. The tube was clamped between the two and opened in microgravity resulting in a vapour diffusion style of crystallization method. On re-entry the payload experienced a 13g force culminating in a 60g jolt when the parachute opened. A total of 101 samples were flown of seven different proteins. The microgravity crystals generally diffracted to equal or higher resolution (five out of seven samples) than the ground controls grown in the same apparatus, and had a greater volume (six out of seven samples) (Plass-Link 1990). Crystals grown under optimal conditions on the ground in standard laboratory apparatus were better than the microgravity or ground-controls.

Large-scale temperature based protein crystallization was first performed on STS-37, April 1991. The Protein Crystallization Facility (PCF) (Long *et al* 1994, 1996) consisted of four cylinders containing 20–500 ml of solution each, over which a temperature gradient could be established.

The first flight to have maintenance of a microgravity environment as its primary mission was the International Microgravity Laboratory (IML-1) on board STS-42 (Janurary 22–30, 1992). This mission carried both the German Cryostat hardware and VDA. Cryostat has two thermal enclosures, each with seven growth cells for liquid–liquid diffusion experiments. Satellite Tobacco Mosaic Virus grown in the thermal enclosures resulted in a 1.8 Å structure (Larson *et al* 1998). The first crystallization experiments conducted by a person mixing solutions in orbit was on STS-50 (June 25–July 9, 1992). It carried the VDA and a glovebox experiment, operated by mission specialist Dr Larry DeLucas, enabling iterative techniques for macromolecular crystal growth in microgravity (DeLucas *et al* 1994).

The first macromolecule crystallization experiments on the Russian Space Station Mir came in 1992, when a progress supply rocket carried up a vapour diffusion device (Stoddard *et al* 1991). Chicken egg white lysozyme and D-amino transferase crystals were grown. The size and diffraction characteristics of the crystals were superior to those grown using identical hardware on the Earth. Using standard laboratory techniques to grow similar crystals on the Earth the improvement was small but still measurable (Stoddard *et al* 1991).

The Spacehab-1 mission (STS-57, June 21–July 1, 1993) retrieved the European Retrievable Carrier (EURECA) long duration satellite launched almost a year earlier on STS-46 (July 31–August 8, 1992) and flew ESA's Advanced Protein Crystallization Facility (APCF). Each APCF contained 48 individual growth cells that could operate in a dialysis, liquid–liquid or vapour diffusion geometry. The facility was temperature controlled to ± 0.1°C and allowed CCD video observation of 12 of the experiments, see section 7.1 (Chayen *et al* 1997, Snell *et al* 1997a, Boggon *et al* 1998). Two APCF facilities flew on STS-65 (July 8–23, 1994), the Second International Microgravity Laboratory (IML-2).

Stoddard *et al* (1991) developed a new vapour diffusion device (VD) reproducing sitting drop vapour diffusion crystallization techniques rather than the hanging drop geometry mimicked by VDA. This flew on Mir from December 1989 to February 1990. The design was further developed into the Protein Crystallization Apparatus for Microgravity (PCAM) (Carter *et al* 1999b). This first flew as a hand held device on STS-62, (March 4–18, 1994), and evolved into the current design that has flown on seven Space Shuttle missions to date.

An experiment named the Gaseous Nitrogen-Dewar (GN2) (Koszelak *et al* 1996) first flew on STS-71 (June 27–July 7, 1995), the first Shuttle Orbiter docking with Mir. Experimentally, the precipitant solution was loaded into Tygon tubing sealed at one end, frozen, then the protein solution added, frozen again and the tube sealed. The frozen sample was transferred to a liquid nitrogen dewar which was launched and transferred to Mir. Over time the liquid nitrogen evaporated, the dewar warmed, and the samples thawed allowing crystallization by free interface diffusion. On this mission GN2 contained 183 samples of 19 proteins (spanning a range of molecular weights, functions and physical properties).

The third Shuttle Orbiter mission to Mir, STS-76 (March 22–31, 1996) introduced the Diffusion-controlled Crystallization Apparatus for Microgravity (DCAM) (Carter *et al* 1999a). This experiment was transferred to Mir to be swapped out on the later, STS-79 mission (September 16–26, 1996). DCAM consists of two cells containing protein and precipitant solutions, separated by a gel plug that controls the equilibration rate. It requires no activation or deactivation by the crew.

There have been a number of crystallization reports from experiments conducted on the ISS (Barnes *et al* 2002, Berisio *et al* 2002, Ciszak *et al* 2002, Kranspenharr *et al* 2002, Nardini *et al* 2002, Vallazza *et al* 2002, Vergara *et al* 2003, Vahedi-Faridi *et al* 2003b). *Escherichia coli* manganese superoxide dismutase (MnSOD) crystals grown on the ISS during the period of December 2001 to April 2002 were 80 times greater in crystal volume than earth-grown crystals. Diffraction spots to 1.26 Å resolution were observed providing significantly improved data than that obtained from crystals grown in Earth laboratories (Vahedi-Faridi *et al* 2003b). Crystals of thaumatin were grown on the ISS in September–October of 2000 (STS 106 mission), synchrotron diffraction data collected from the best space-grown crystal extended to 1.28 Å compared to the best ground control crystal at 1.47 Å (Barnes *et al* 2002).

Kundrot *et al* (2001) report that, prior to STS-95, 20% of macromolecules flown obtained their highest diffraction resolution to date from the microgravity crystals. However, if the analysis is limited to those proteins that flew four or more times the success rate based on the criteria of improved diffraction resolution increases to 60%. Known results from experiments on the Space Shuttle Orbiter are summarized in figure 9 (Judge *et al* 2005).
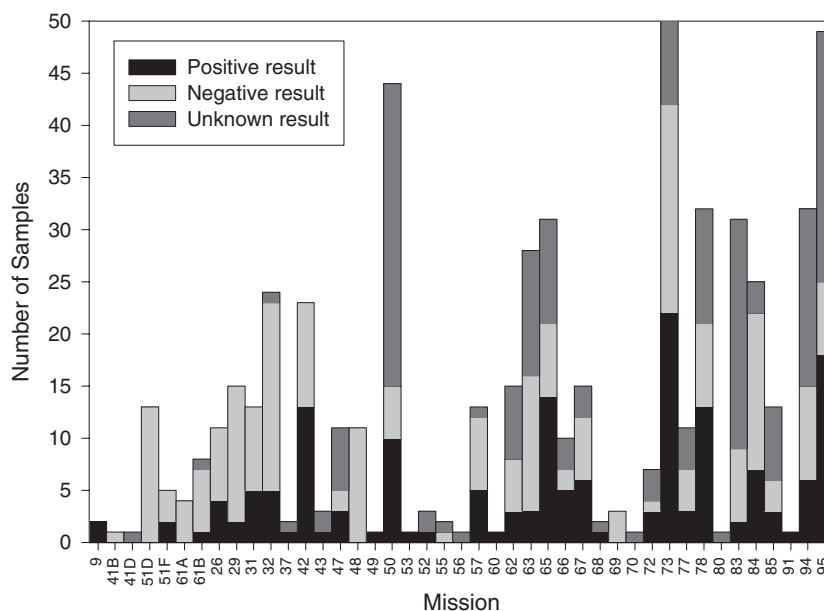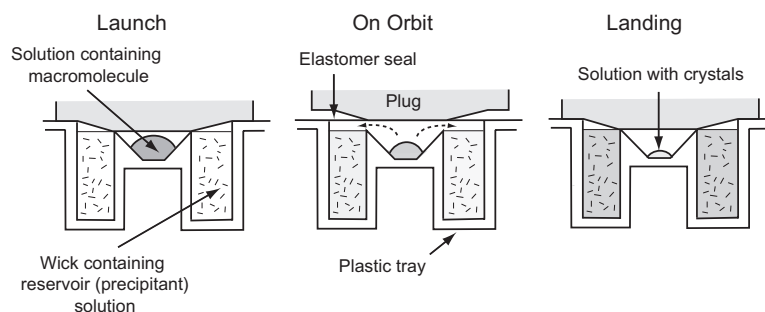
Figure 9. Plot of experimental reports per mission in chronological order. In most cases each sample represents several individual crystallization experiments. Positive results (improvement) appear on the bottom with negative then unknown stacked above that, respectively. For mission STS-73 the bar for unknown results has been truncated as reports from 19 samples on this mission were not available primarily as the experimental purpose was to test crystallization hardware rather than to grow and analyse the crystals. Mission STS-50 also has a large number of unknown results due to samples being used in a glove box experiment to test sample manipulation. Judge *et al* (2005) with the permission of the IUCr.
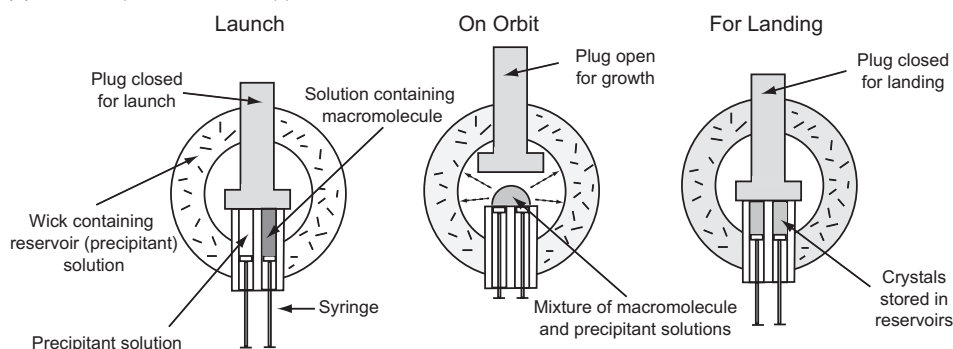
6. Common microgravity apparatus

In section 1.1 we described the different methods of crystal growth that are found in the ground-based laboratory. Figure 10 illustrates some of the apparatus that has been developed to adapt these methods for microgravity crystal growth. There are several common features in the apparatus: an activation or delay step so that the crystallization does not begin until the samples reach orbit; activation must be simple or automatic and each apparatus is modular so that many experiments can be set up.

The PCAM (Carter *et al* 1999b) uses the vapour diffusion method of growth, figure 10(*a*). Each experiment is conducted in one chamber of a 'puck' containing seven chambers in total. These pucks are arranged nine to a cylinder and typically carried in sets of six cylinders inside a thermally controlled carrier for a total of 378 individual experiments. Each chamber is filled with a macromolecule solution volume of between 10 and 40 μl. An elastomer seal is pushed down by a plug to seal the macromolecule solution from the precipitant reservoir (held in a porous wick). When orbit is established this plug is retracted allowing the solutions to come into vapour contact. For return to Earth the plug is pushed back sealing the separate chambers again. The individual 'pucks' can then be directly taken to an x-ray source for crystal extraction and analysis. Vapour diffusion crystallization is also accommodated in the VDA (DeLucas *et al* 1986) shown in figure 10(*b*). This consists of a syringe with two barrels holding the macromolecule and precipitant solution. To activate crystallization in orbit a plug above this syringe is lifted and the syringes activated to extrude the solutions into a crystallization
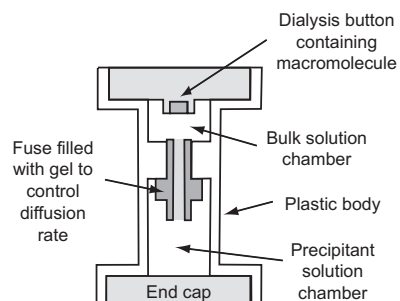
(a) PCAM : Protein Crystallization Apparatus for Microgravity

Launch   On Orbit   Landing

Solution containing
macromolecule

Elastomer seal

Plug

Solution with crystals

Wick containing
reservoir (precipitant)
solution

Plastic tray

(b) VDA : Vapour Diffusion Apparatus

Launch   On Orbit   For Landing

Plug closed
for launch

Solution containing
macromolecule

Plug open
for growth

Plug closed
for landing

Wick containing
reservoir (precipitant)
solution

Syringe

Precipitant solution

Mixture of macromolecule
and precipitant solutions

Crystals
stored in
reservoirs

(c) DCAM : Diffusion-controlled Crystallization
Apparatus for Microgravity

(d) EGN : Enhanced Gaseous Nitrogen Dewar

Dialysis button
containing
macromolecule

Fuse filled
with gel to
control
diffusion
rate

Bulk solution
chamber

Plastic body

Precipitant
solution
chamber

End cap

(i) Uniform (batch)

(ii) Two phase

(iii) Three phase

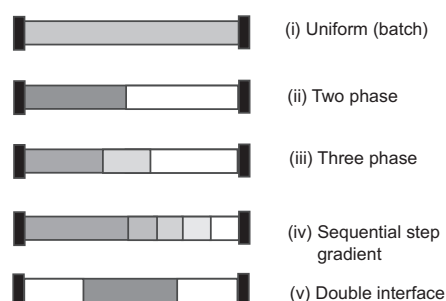(iv) Sequential step
gradient

(v) Double interface

Figure 10. Schematic illustration of the operation of the most common apparatus used for microgravity crystallization experiments. The diagrams are not to scale.

chamber surrounded by a porous wick containing precipitant solution. In later variants of the apparatus a third syringe barrel was provided to mix solutions. A total of 20 of these chambers were housed in a single experimental tray with four trays accommodated in a thermally controlled carrier giving a total of 80 experiments. Experiment samples typically had between 20 and 40 μl macromolecule volume in the syringes and 1 ml of precipitant contained in the reservoir.

A larger volume apparatus is the DCAM (Carter *et al* 1999a), figure 10(*c*). This operates by a diffusion of precipitant into a dialysis button containing the macromolecule solution (50 μl volume). For larger crystals the bulk solution chamber can be filled with the macromolecule

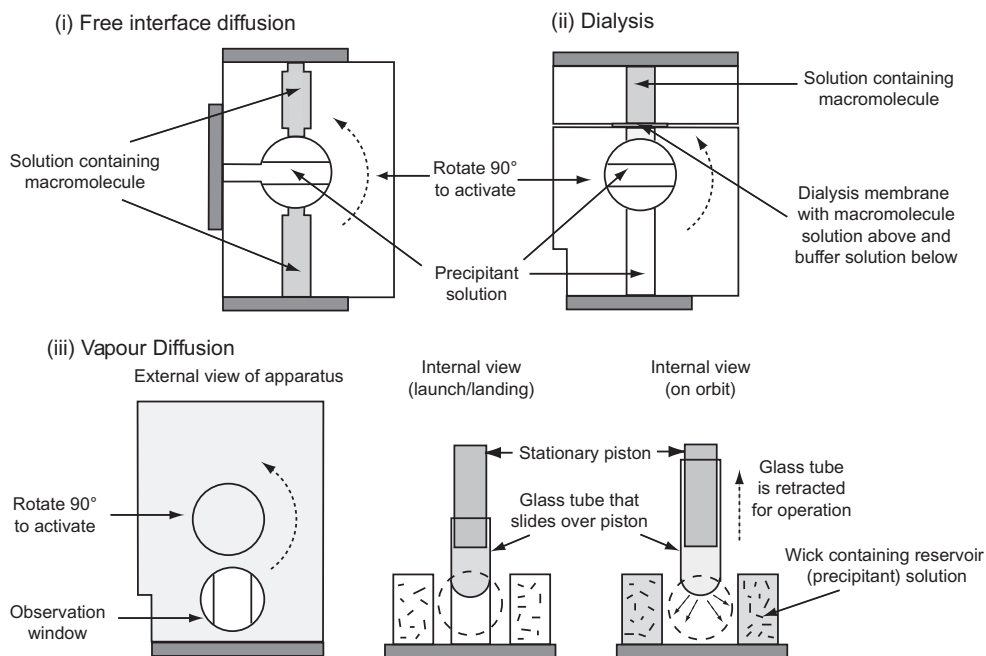(e) APCF : Advanced Protein Crystallization Facility

Figure 10. (Continued.)

solution (2 ml volume). The rate of diffusion is controlled by the length and material in a gel fuse. The precipitant solution is stored on one side of this fuse with the macromolecule solution on the other. A total of 81 experiments can be accommodated in a thermally controlled carrier. A variant on the diffusion crystallization method is the Enhanced Gaseous Nitrogen Dewar (EGN) (Koszelak *et al* 1996). This makes use of tygon tubing containing crystallization experiments in a frozen state. The experiments can be set up in many different ways, figure 10(*d*). Each experimental solution is filled, frozen, then the next solution added. Finally the tubing is sealed. The experiments are stored at $-80°$C and rely on a slow thawing of the solutions after orbit is established as the dewar containing them is allowed to come to ambient temperatures. A typical experiment uses 1.6 mm diameter, 85 mm length tygon tubing giving a useable volume of $\sim$150 μl. Smaller volumes are available through tubing size and partial filling. A dewar accommodates approximately 500 experiments.

The ESA has developed the APCF (Snyder *et al* 1991, Bosch *et al* 1992) which uses modular experiment chambers, figure 10(*e*). Three types of crystallization are accommodated, free interface diffusion, dialysis and vapour diffusion. All are activated in orbit and deactivated on return by a 90° rotation of a drive cylinder. For free interface diffusion the rotation brings two chambers containing the macromolecule solution and a precipitant chamber into line. For dialysis the rotation connects the precipitant chambers with the macromolecule chamber across a dialysis membrane. Both the free interface diffusion chamber and the dialysis chamber are made of quartz glass allowing observation of the experiment through a video microscope. The free interface diffusion chamber comes in several sizes and can accommodate macromolecule solution volumes from 20 to 1280 μl with a total volume of between 250 and 4420 μl. The dialysis chamber accommodates macromolecule solutions from 4 to 80 μl with a total volume of 700 μl. The vapour diffusion chamber uses a glass tube containing the

macromolecule solution that is retracted on establishing orbit to allow the solution to come into vapour contact with the precipitant contained in a porous wick. For landing the tube is put into position again to separate the solution with crystals and the precipitant wick. The vapour diffusion chamber is opaque with the exception of a window allowing viewing of the crystallization experiment. Two types of vapour diffusion chamber are available allowing small volume, 4–8 μl, and larger volume drops, 35–80 μl, of macromolecule solution. The precipitant volume contained in the wicks is 700 μl. The APCF apparatus was designed with both a crystal production capability and a diagnostic experiment capability. The APCF provides its own thermal control in a thermal container with each containing four experiment stacks made up of 12 chambers for a total of 48 experiments in each APCF.

Not shown is the commercial PCF (Long *et al* 1994, 1996) which uses the variation in solubility as a function of temperature to control growth. Crystallization solutions are contained premixed at a temperature where the macromolecule is soluble. In orbit this temperature is actively controlled to reduce the solubility and produce crystals. Crystallization is large scale with a range of sample volumes from 50 to 500 ml.

7. Analysis methods applied to microgravity experiments

Crystallization experiments in microgravity can be categorized as either for fundamental studies of crystal growth mechanisms, or for the production of diffraction quality crystals for structural data collection, or a combination of both.

Fundamental studies aim to understand the crystallization process and how that process can be optimized in microgravity. Analysis of the results requires control experiments to isolate the effects associated with the reduced acceleration. Ideally two types of control are needed, first identical apparatus, biochemicals, duration, temperature, etc and second another control using the apparatus and conditions that produces the best crystals in the ground-based laboratory. This second control is important as apparatus designed to work well in microgravity might not be optimal to produce crystals on the ground.

Growth of crystals in microgravity to provide good structural data does not need as extensive ground control experiments. The best crystals available are already well characterized and for success, an experiment only needs to provide improvement over the previous best results. That said, the success rates for improvements seen in microgravity are approximately 35% for macromolecules that had more than one flight. Although there is no perceived need then for detailed ground-control experiments when microgravity is used to produce crystals for structural data even basic control experiments do provide useful information to benefit other investigations.

Analysis of experiments can occur at three stages; analysis of the samples before crystallization and preliminary experiments to optimize the use of the hardware, analysis during growth in orbit and analysis of the samples on their return to the ground.

7.1. Analysis before and during crystal growth

Before the experiment it is important to characterize the sample as comprehensively as possible. In addition to a standard biochemical analysis, the effects of storage in the apparatus before activation and delays in returning samples following growth also need to be investigated.

Diagnostic techniques during crystal growth need to be non-invasive and reliable. Optical techniques answer these requirements and include light scattering, interferometry and visual microscopy. Light scattering and interferometry techniques are described extensively elsewhere (Shlichta 1986, Mikol *et al* 1990, Wlison 1990, Ferre-D'Amare and Burley 1994).

Visual observation was used with the first macromolecular crystallization experiment (Littke and John 1984, 1986). It was not used again until the launch of the EURECA on the STS-46 mission (Snyder *et al* 1991, Schmidt *et al* 1992). The blue protein α-crustacyanin was grown and a slow depletion of protein in the growth chamber was imaged (Zagalsky *et al* 1995, Boggon *et al* 1998). The crystals were easily distinguished and remained stable through the mission once formed. Another experiment on the same EURECA mission was the growth of aspartyl-tRNA synthetase (Lorber *et al* 2002). By tracking precipitate formation, the diffusion profile in the chamber was recorded. Analysis of accelerations onboard the mission showed that a maximum of only $62.5\mu g$ was experienced (Eilers and Stark 1993). Unfortunately, EURECA suffered cooling problems before it was retrieved on STS-57 and no crystals were returned for analysis on the ground.

Crystal growth in the APCF facility onboard the space shuttle Orbiter has been monitored using a CCD camera. On the STS-65 mission lysozyme crystallization was monitored with a series of images at different focal lengths taken over a 40 min period, approximately every 8 h (Snell *et al* 1997a). In particular, three crystals in solution were tracked. The speed of the crystal movements were approximately $200\,\mu m\,h^{-1}$ in the same direction for all three crystals covering a total distance of 0.3 mm (i.e. approximately one crystal width). A crystal nucleated attached to the chamber wall, figure 11. Analysis of this crystal every ~ 8 h revealed spurts and lulls in its growth rate directly correlated with those of astronaut exercise periods (Snell *et al* 1997a). Apocrustacyanin C_1 was crystallized by the vapour diffusion method and the crystals were also tracked by CCD video on the same mission. The images were dark and the reader is referred to Chayen *et al* (1997) for the best reproduction but they showed a fairly speedy circular movement of the crystals dependent on the position of the crystal in the drop. These crystals all moved through the drop in a way consistent with that of Marangoni convection (Chayen *et al* 1996, 1997, Savino and Monti 1996, Boggon *et al* 1998).

A number of studies were carried out using the APCF on the STS-78 mission. Otalora *et al* (1999b) studied the use of long thin capillary growth cells and used a Mach–Zehnder interferometer and CCD video observation for diagnostic work, during growth. Maximum growth rates were observed slightly after nucleation with crystal movement seen during the mission. The growth rate did not seem to be correlated with changes in the velocity of the crystal as might be expected if the deformation of the depletion zone was large enough to alter the supersaturation around the crystal.

Table 1 lists visual observations of crystal movements in microgravity experiments. All the observations have been made by the APCF or its predecessor EURECA. Crystals have significant motion during growth in microgravity, except for those grown on the free flying satellite, EURECA.

Another key diagnostic to monitor during crystal growth is the acceleration environment. The microgravity environment of the Space Shuttle Orbiter and the ISS can be measured by a number of accelerometer systems, e.g. the Space Acceleration Measurement System (SAMS) (DeLombard *et al* 1992). An example of this is shown in figure 12 taken from the STS-65 mission (Snell *et al* 1997a). This is produced by a time-domain analysis performed by taking the root mean square of the data from three axes followed by computing the sum of squares. The data is combined into a single vector and then presented in the frequency domain by computing successive power spectral densities and assigning a colour to the base 10 of the power spectral density intensity. Analysis of gravitational accelerations onboard the Orbiter showed that astronaut exercise periods, especially the use of an ergometer (a bicycle type device), produced periods of g-jitter approaching $1000\mu g$. It seems that the increased gravity of these periods induced acceleration within the crystallization chamber allowing convective
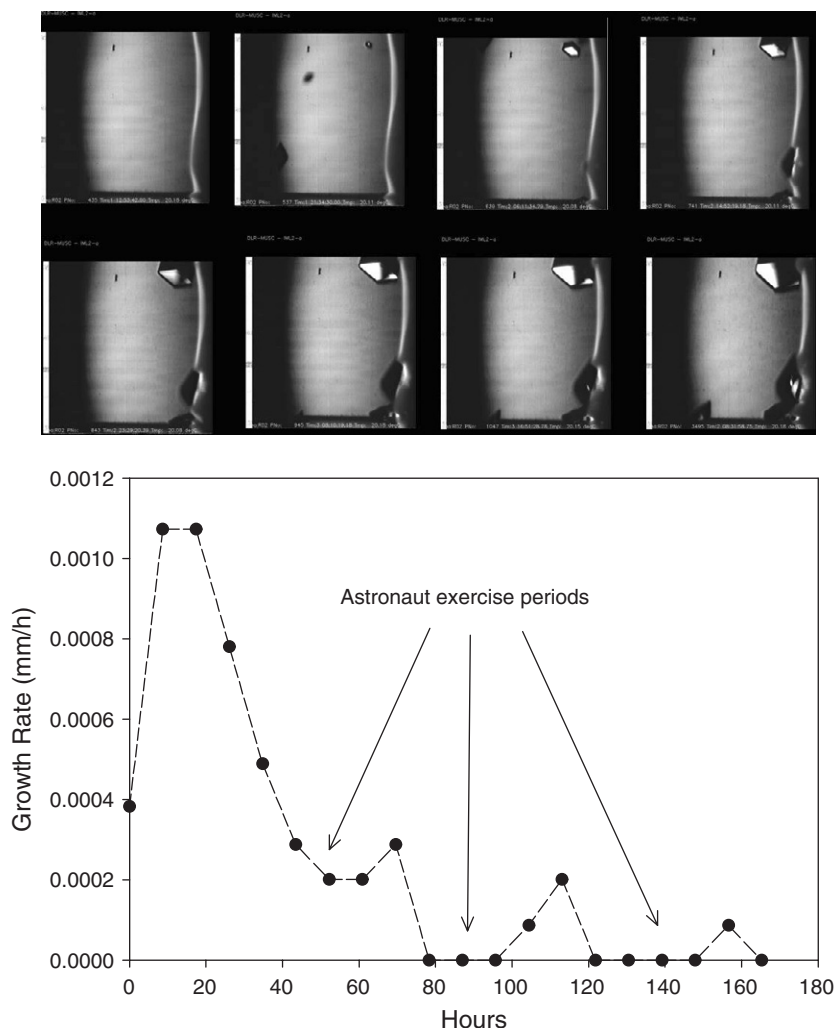
Figure 11. CCD video images of a single microgravity-grown tetragonal lysozyme crystal (top right of each image) starting at 36 h, 54 min (top left) through to 296 h and 32 min (bottom right) taken using the APCF on the STS-65 mission (Snell *et al* 1997a). The 110 face of the crystal is clearly visible. The vertical slightly curved line to the right of the crystal is the dialysis membrane and some other crystals are visible growing on the membrane. Below this is a plot of growth rate as a function of time with astronaut exercise periods noted.

buoyancy to break down the depletion zone thus transporting new protein to the growing crystal faces (Snell *et al* 1997a), figure 11.

7.2. Analysis of the resulting crystals

Diffraction measurements are the optimum measure of crystal quality, however a crystal may look like visually. There are several types of physical x-ray diffraction analyses now employed in addition to standard diffraction data collection for structural studies, e.g. reflection profiling, topography and reciprocal space mapping (Snell *et al* 2003). Reflection profiling can be

Table 1. Experimental speeds and distances travelled of microgravity-grown protein crystals for published cases. Notes; (1) The movement of crystals, for a 7-week period was <1–2 pixels (i.e. <25–50 μm); thereafter problems with the cooling elements caused crystal movements, (2) instantaneous speed for all crystals over the time periods: (a) Mission Elapsed Time (MET) 3/02:35 to 3/04:47, (b) = MET 4/04:48 to 4/06:31, (c) = MET 6/01:18 to 6/03:01.

Mission	Protein	Crystallization method	Time period	Crystal speed (μm s^{-1})	Total observed crystal movement	Notes	References
Spacehab (STS-57)	Lysozyme	Dialysis	3 days 2 h	0.5	—	1	(Garcia Ruiz and Otalora 1997, Ries-Kautt et al 1997).
Spacehab (STS-57)		Dialysis			Sudden after growth		(Weisgerber and Helliwell 1993)
IML-2 (STS-65)	Apocrustacyanin C_1	Vapour diffusion	8 min 45 s	2.1	1.08 mm		(Boggon et al 1998, Chayen et al 1997)
IML-2 (STS-65)	Lysozyme	Dialysis	40 min	0.05	0.3 mm		(Boggon et al 1998, Snell et al 1997a)
EURECA	α-crustacyanin	Free interface diffusion	7 weeks	0	0		(Boggon et al 1998, Zagalsky et al 1995)
USML-2 (STS-73)	Thaumatin	Free interface diffusion	7.5 days	0.005	—		(Lorber et al 2000)
LMS (STS-78)	Lysozyme	Dialysis	24–260 h	0.004	0.42–3.38 mm		(Boggon et al 1998)
			2 h	0.026	0.21 mm	2(a)	
			2 h	0.027	0.17 mm	2(b)	
			2 h	0.031	0.19 mm	2(c)	
LMS (STS-78)	Lysozyme	Free interface diffusion	28 h	40 μm hr^{-1} (max)	0.1 mm (average)		(Otalora et al 1999b)
LMS (STS-78)	Thaumatin	Dialysis	11.5 days	0.009	—		(Lorber et al 2000)
STS-95	Lysozyme	Free interface diffusion	170 h	0.007	—		(Garcia Ruiz et al 2001)

carried out similar to standard structural data collection with the only difference being the minimization of instrument and beam contributions and fine step crystal rotation (Colapietro et al 1992, Fourme et al 1995, 1999, Snell et al 1995, Bellamy et al 2000, Boggon et al 2000). At the synchrotron the spectral parameters are controlled by the monochromator and the x-ray beam divergences are controllable via precision slits in the vertical and horizontal planes finally limited by the intrinsic properties of the synchrotron machine electron beam emmitance. Reflection profiling can also be accommodated in the laboratory, at the expense
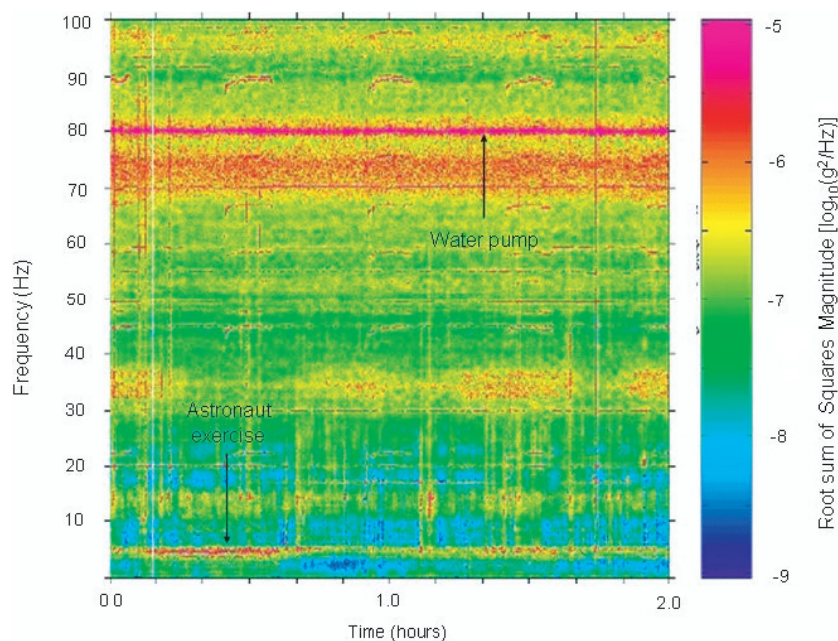
Figure 12. Spectrogram of SAMS data showing astronaut exercise in a 30 min interval at 5 Hz and the continuous operation of a water pump at 80 Hz. Many other features of the acceleration noise on a space shuttle mission are also seen in the data (Snell *et al* 1997a).

of flux, using a Bartels 4 bounce monochromator (Bartels 1983, Hu *et al* 2001). Topography uses a similar optics set-up but with a spatially sensitive detector, e.g. photographic film, so that the detail in the reflection can be resolved (Stojanoff and Siddons 1996, Stojanoff *et al* 1996, 1997, Dobrianov *et al* 1998, Fourme *et al* 1999, Otalora *et al* 1999a, Boggon *et al* 2000). Finally in reciprocal space mapping, an additional crystal is inserted between the sample and the detector allowing the reciprocal lattice to be resolved in two dimensions, see section 8.2 (Fewster 1997, Volz and Matyi 1999, 2000, 2001, Boggon *et al* 2000).

The physical quality of macromolecular crystals resulting from microgravity experiments has proved to be so high that care needs to be taken that the instrument and geometrical effects do not mask the crystal properties under study (Greenhough and Helliwell 1982, Helliwell 1988, Colapietro *et al* 1992, Bellamy *et al* 2000, Snell *et al* 2003). The analysis techniques can be divided into properties that are measured from single reflections, a statistical sample of reflections or as complete a data set as possible.

7.2.1. Single reflection techniques. Single reflection techniques include topography, described above, which is a technique that provides useful but still somewhat qualitative information. A topograph is a detailed image of those parts of the crystal contributing to the reflection at a single Bragg angle (Stojanoff and Siddons 1996, Stojanoff *et al* 1997). For a perfect crystal the whole crystal contributes to the Bragg reflection over an infinitely small Bragg angle. No crystal is perfect, and, typically, for a high-quality crystal distinct regions of the crystal produce contrast at slightly differing Bragg angles. For poor quality crystals the topograph appears grey, the contribution of different parts of the crystal at different Bragg angles are smeared out.

A single reflection can also provide an indication of the crystal mosaicity but is most useful when comparing identical reflections in a sample population of crystals as anisotropic effects may be present; as a minimum, reflections at or near to identical Bragg angles must be compared. Implicitly a reduction in mosaicity implies an increase in signal-to-noise for identical reflections from otherwise identical crystals. Figure 3 shows crystals as being made up of distinct domains according to the Darwin model and illustrates how physical features described by the mosaic model can be seen in the reflection-profile (rocking width) measurements. All of the effects can be anisotropic. The analysis of individual reflections provides a measure of the long-range order within the crystal. In addition, by making measurements in multiple regions of reciprocal space, crystal anisotropy can be investigated. Note, reflection analysis does not provide information about short-range disorder, see figure 2.

7.2.2. Statistical techniques. A statistical sample of reflections, i.e. a partial or complete diffraction data set, allows the overall reflection width, the diffraction resolution at a defined signal-to-noise ($I/\sigma(I)$ usually $\geqslant 2$), and statistical agreement between the intensity of symmetry related reflections (termed R_{merge}) to be used as indicators of quality. R_{merge} is defined as:

$$R_{\mathrm{merge}} = \frac{\sum_{hkl} \sum_i |E_i(hkl) - \overline{E(hkl)}|}{\sum_{hkl} \sum_i E_i(hkl)}, \tag{7.1}$$

where E_i is the intensity of a reflection from the (h, k, l) plane. The use of R_{merge}, diffraction resolution, signal-to-noise ratio and completeness is described by Weiss (2001). The resolution at a defined signal-to-noise is dependent on the crystal, the beam illuminating it, the data collection protocol and the detector properties. This measure is useful to compare when the same experimental set-up and protocol are used for experiments but requires careful control of all these parameters. R_{merge} is inherently dependent on the redundancy of the data and other statistical measures which correct for this are available (Weiss 2001). Arai *et al* (2004) have proposed the use of a relative Wilson plot as a quality indicator. The relative Wilson plot normalizes the data against a reference crystal. The quality of any crystal relative to the reference crystal is given by the sign and the magnitude of the gradient of the slope from the resulting relative Wilson plot. This is a useful technique for comparison within a given population of crystals but again, as in the case of resolution, requires careful control of all the experimental parameters.

7.2.3. Complete diffraction data sets. Diffraction data collection for macromolecular crystal structure determination are well described in various textbooks (Drenth 1999, Rossmann and Arnold 2001, Blow 2002, Giacovazzo 2002). Specifics to synchrotron radiation are described in Helliwell (1992).

The structural solution, refinement and resulting detail seen in the electron density maps is the ultimate measure of crystal quality. Unfortunately, in terms of understanding and optimizing crystal growth the effort needed to provide feedback of this nature is substantial. This type of assessment is useful for understanding the growth process at an intermolecular level. In order to compare crystals of the same molecule and thereby evaluate differences in overall *B* factor of the crystals the relative *B* factor calculation between two crystals basically removes the complication of the molecular transform detailed shape, and therefore is calculable at less than atomic resolution. This assumes of course that the protein structure basically remains the same from crystal to crystal; in some cases protein molecule flexibility can lead to some variability.

So, for two crystals, labelled 1 and 2, the Wilson equation (1.5) can be rewritten as:

$$\frac{E_{\mathrm{obs}}(h,k,l)_1}{E_{\mathrm{obs}}(h,k,l)_2} = \mathrm{e}^{(-2(B_2-B_1)\sin^2\theta/\lambda^2)} \tag{7.2}$$

and thus a plot of $\log(E_{\mathrm{obs}}(h,k,l)_1/E_{\mathrm{obs}}(h,k,l)_2)$ has a gradient of $-2(B_2-B_1)$. This is the so-called relative Wilson plot and has been used in the analysis of a number of microgravity-grown crystals to compare them to ground-grown controls (DeLucas *et al* 1989, 1991, 1994, Koszelak *et al* 1995). For identical crystals the slope is zero, if one crystal is improved over the other the slope is non-zero.

Good examples of the development of diagnostic methods for analysing the crystals are given in section 8. These cover the development of single reflection techniques through to complete data sets.

8. Case studies and examples

There are a number of good examples of microgravity crystallization experiments including the development of analysis methods, the application of those methods and the resulting structural knowledge obtained. The perfection of crystals, and the potential improvement via microgravity and other crystal growth techniques, is a recurrent theme.

8.1. Microgravity experiments providing new structural data

Figure 13 shows a selection of macromolecular structures that have been improved from microgravity experiments. Further detail on the diffraction resolution improvement in these structures is given in table 2 and the reader is referred to the appropriate reference for details on the structural information that resulted and the biological implications.

8.2. Development of crystal diagnostic methods with lysozyme

Lysozyme, an enzyme that breaks down bacterial cell walls, reproducibly crystallizes under a wide range of conditions. It has been extensively studied, on the ground and in microgravity, due to its crystallization properties and that it is commercially available at high purity and low cost.

Lysozyme was crystallized on the Spacehab-1 mission, STS-57. The crystals produced were visually comparable (average length 0.7 mm) with those grown in identical apparatus on the ground. Rocking width profiling was used to examine crystals grown in microgravity, first suggested by Helliwell (1988). This was accomplished with x-ray analysis of the crystals at the Daresbury Synchrotron Radiation Source using the Laue method in an ultra-long distance camera mode (Snell *et al* 1995, Helliwell *et al* 1996). Laue diffraction spot sizes were measured from three microgravity-grown and two earth-grown crystals. The spot sizes were converted to mosaic spread values using the formula:

$$\Delta_{\mathrm{radial}} = \frac{2\eta D}{\cos^2 2\theta}, \tag{8.1}$$

where Δ_{radial} is the Laue radial spot size with the direct beam size deconvoluted out, D is the crystal to film distance and θ the Bragg angle (Andrews *et al* 1987). The mosaicities of the crystals grown in microgravity were on average 0.0015° and the earth-grown crystals 0.0047°.

A similar experiment was conducted for crystals from the STS-65 mission. The microgravity-grown crystals were on average 1.8 mm in length (with the longest being 2.5 mm) in comparison to the ground-grown crystals which averaged 0.8 mm in length. Station A of the
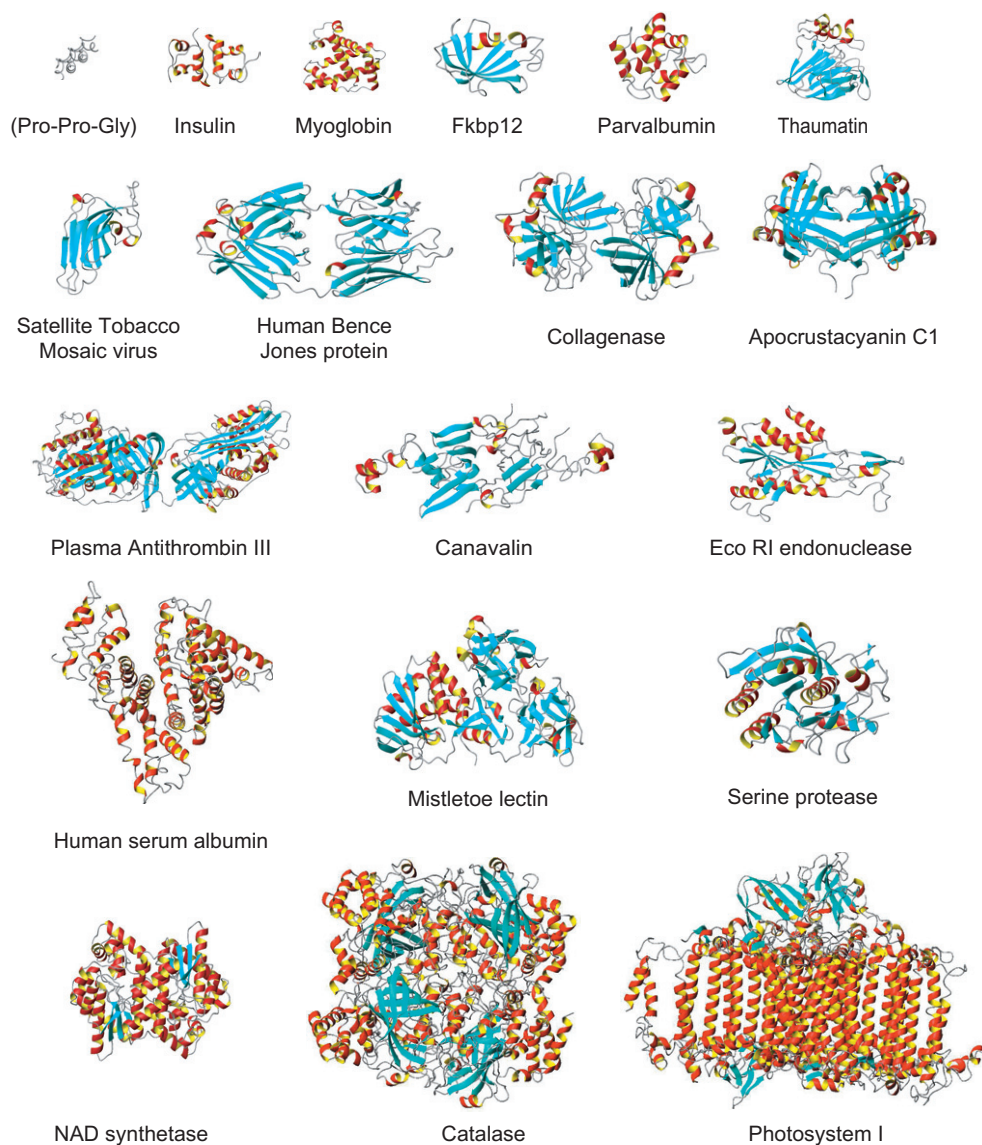
Figure 13. Ribbon diagrams of a selection of macromolecular structures that have been improved by crystallization experiments in microgravity. Images are not to relative scale. References are given in table 2.

Swiss/Norwegian beamline at the European Synchrotron Radiation Facility (ESRF) was used with a Huber φ-circle diffractometer and a monochromatic beam. The station was unfocused and positioned 45 m from the source giving an instrument resolution function (Colapietro *et al* 1992) of 0.00195°. Detailed examination of identical reflections from one of the earth-grown and a microgravity-grown crystal took place. The results were dramatic; after deconvolution of the instrument and spectral contribution the earth-grown crystal exhibited mosaicities ranging from 0.0067° to 0.0169° (average 0.0120°) measured at full-width at half-maximum (FWHM) while the microgravity crystal exhibited mosaicities from 0.0017° to 0.0100° (average 0.0047°).

Table 2. Structures deposited in the PDB resulting from microgravity experiments: [(Pro-Pro-Gly)$_{10}$]$_3$ (Berisio *et al* 2002); Insulin (Smith *et al* 2003), Myoglobin (Miele *et al* 2003), Fkbp12 (Wilson 1995), Parvalbumin (Declercq *et al* 1999), Satellite Tobacco Mosaic Virus (Larson *et al* 1998), Apocrustacyanin C$_1$ (Habash *et al* 2003), Human Bence Jones protein (Alvarado *et al* 2001, Terzyan *et al* 2003), Plasma Antithrombin III (Skinner *et al* 1997), Canavalin (Ko *et al* 2001), Collagenase (Broutin-L'Hermite *et al* 2000), Human serum albumin (He and Carter 1992), Mistletoe lectin (Kranspenharr *et al* 2002); Serine protease (Betzel *et al* 2001), Catalase (Ko *et al* 1999); NAD synthetase (Symersky *et al* 2002), Photosystem I (Klukas *et al* 1999), Nucleosome core particle (Harp *et al* 2000), Alcohol dehydrogenase (Esposito *et al* 2002) and Bacteriophage lambda lysozyme (Evrard *et al* 1998).

Macromolecule	Molecular weight (Da)	Resolution (Å) Ground	Resolution (Å) Microgravity	PDB identifier	Apparatus	Method	Mission
[(Pro-Pro-Gly)$_{10}$]$_3$	8000	1.60	1.30	1K6F	APCF	DIA	STS-95
Insulin	6000	—	1.00	1MSO	PCF	Temp	STS-95
Myoglobin	17 000	1.60	1.04	1NAZ	HDPCG	VD	ISS 6A and 8A
Fkbp12	11 800	~1	2.20	1FKK	VDA	VD	STS-50
Parvalbumin	11 390	1.75	0.91	2PVB	PCAM	VD	STS-83
Satellite Tobacco Mosaic Virus	1 400 000	2.3	1.80	1A34	CRYOSTAT	FID	STS-42
Apocrustacyanin C$_1$	20 600	2.00	1.85	1OBQ	APCF	VD	STS-78
Human Bence Jones protein	22 600	—	1.95	1LGV	LMA	VD	STS-95
Plasma Anththrombin III	58 000	3.00	2.60	2ANT	PCAM	VD	STS-67
Canavalin	145 000	2.60	1.70	1DGW	APCF	FID	STS-65
Collagenase	25 209	1.80	1.70[1]	2HLC	APCF	VD	STS-65
Eco RI Endonuclease	31 000	3.0	2.70	1ERI	PCAM	VD	STS-85
Human serum albumin	67 000	—	2.80	1UOR	VDA	VD	STS-42
Mistletoe lectin	27 800	2.3	1.90	1M2T	HDPCG	VD	STS-105
Serine protease	45 000	1.30	0.98	1IC6	APCF	VD	STS-95
Catalase	240 000	2.50	2.20	4BLC	EGN	FID	MIR
NAD synthetase	60 000	(1.95)	(1.47) 1.0	1KQP	VDA	VD	STS-95
Photosystem I	1 200 000	—	4.0	1C51	APCF	DIA	STS-73 and 78
Nucleosome core particle	206 000	~2.9[2]	2.50	1EQZ	DCAM	DIA	STS-73
Alcohol dehydrogenase	38 000	2.50	1.85	1JVB	APCF	DIA	STS-78
Bacteriophage lambda lysozyme	17 800	—[3]	2.30	1AM7	PCAM	VD	STS-67

Notes: 1. Although only a minor improvement in resolution, the authors report that the overall improvement in signal-to-noise resulted in an 'amazing improvement in quality' for the electron density maps. 2. The authors do not list the resolution of the ground sample but estimate it from pseudoprecession images. 3. The authors do not report data for the ground-grown crystal, only that the microgravity sample diffracted better.

Deconvolution of the instrument and spectral contributions made use of the relationship;

$$\eta = (\varphi_R^2 - \mathrm{IRF}^2)^{1/2}, \tag{8.2}$$

where η is the deconvoluted mosaicity, φ_R the measured rocking width and IRF the instrument resolution function. The integrated intensities of the microgravity-grown crystal reflections were approximately double those of the earth-grown crystals which corresponded to the almost doubling in volume. However, the dramatic effect was in the eight-fold increase in peak height. The reduction in mosaicity caused a corresponding increase in signal-to-noise. Figure 14 shows an example of one of the reflection profiles from a microgravity- and an earth-grown crystal and a 1.2 Å resolution reflection observed only in the case of the microgravity-grown crystal.
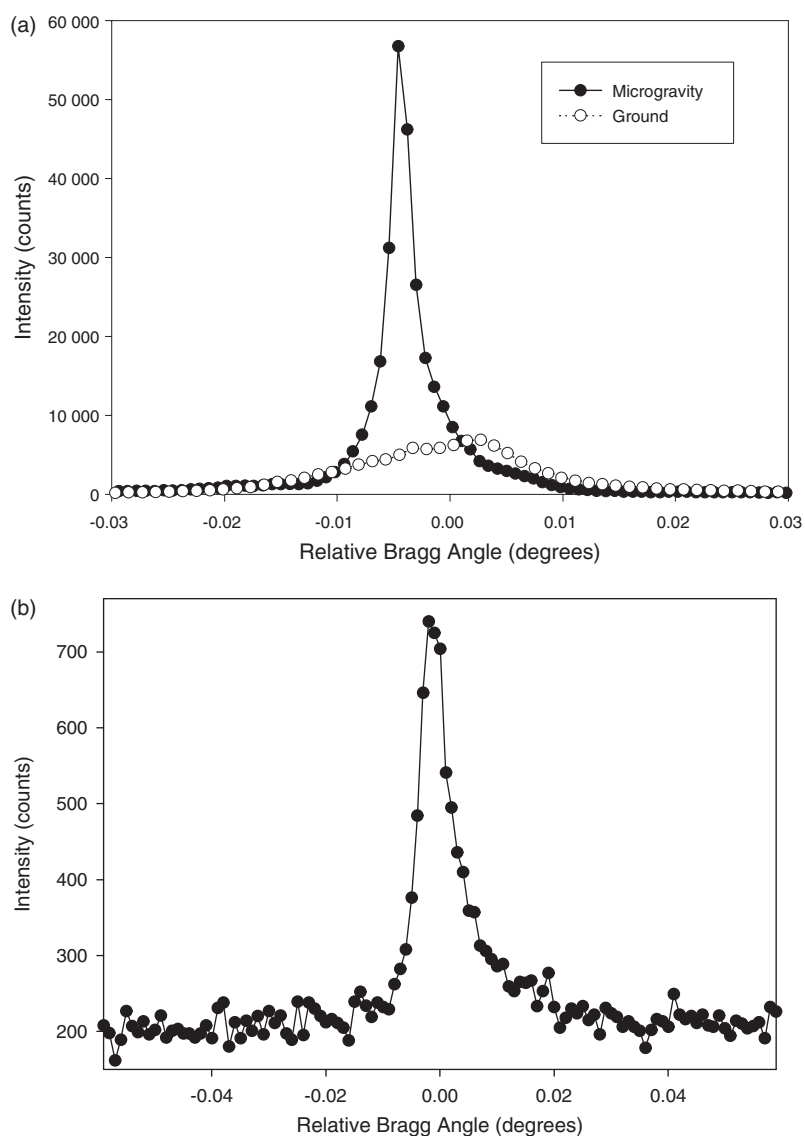
Figure 14. Rocking width profile for (*a*) an identical reflection from microgravity-grown and ground-grown lysozyme crystals (only every second data point is shown for clarity) and (*b*) a 1.2 Å resolution reflection observed only in the microgravity-grown crystal case (note that the signal-to-noise is about 4 at this resolution implying that diffraction data to higher resolutions is still available).

Another technique used to examine the microgravity-grown crystals was x-ray topography. Topography is an ideal measurement to complement mosaicity analysis requiring essentially similar x-ray beam characteristics. The combination of mosaicity analysis with topography in the case of macromolecular crystals was first suggested by Shaikevitch and Kam (1981). Fourme *et al* (1995) examined a ground-grown lysozyme crystal using this combination of methods illustrating three domains within the crystal. Analysis of microgravity-grown lysozyme crystals from the STS-65 mission with topographs, (Snell 1995, Chayen *et al* 1996,
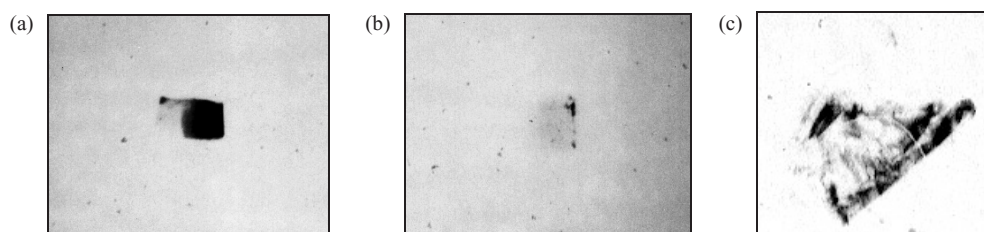
Figure 15. Topographs from (*a*)–(*b*) a microgravity-grown lysozyme crystal, 1.1×0.9 mm in projection and (*c*) shown further enlarged, an earth-grown lysozyme crystal 0.8×0.6 in projection (Boggon *et al* 2000).

Stojanoff *et al* 1996) shows large areas of uniform contrast (either light or dark) indicative of high order and therefore quality, figures 15(*a*) and (*b*). The boundary between different areas of contrast is also sharp. Ground-grown, control crystals displayed a 'crumbly' grey appearance with small regions of contrast, figure 15(*c*).

Ng *et al* (1997) grew thaumatin on two Space Shuttle missions, STS-73 and STS-78, using the APCF. There was a clear increase in the largest size of crystals grown by dialysis methods in microgravity compared to those grown on the ground. The average and largest sizes of crystals seemed dependent on the macromolecule concentration. The overall x-ray intensity as a function of resolution was increased for the microgravity crystals yielding a higher resolution, 1.5 Å versus 1.7 Å and nearly 30% more diffraction intensities above 3σ for the entire data set. Mosaicity studies were also used to analyse these crystals. The FWHM of Guassian fits of the reflection profiles of microgravity- and earth-grown crystals averaged 0.010° versus 0.047°, respectively. The signal-to-noise of the data from the microgravity crystals was increased.

Apocrustacyanin C_1 was grown in the APCF on the STS-65 mission and was monitored by CCD video. Several single rod-shaped crystals were obtained. The video images showed a movement of crystals in the drop over time consistent with Marangoni convection (Savino and Monti 1996). Thus, the benefit of microgravity establishing a stable depletion zone around the growing crystal was violated. X-ray analysis of the resulting apocrustacyanin C_1 crystals required the development of an anisotropic mosaicity analysis and a rocking-volume plot. The lowest mosaicity consistently occurred along the *h* axis correlated with the smallest cell parameter '*a*' and the longest dimension seen in the crystals (Snell *et al* 1997b). The conclusion of these evaluations was that a partial improvement of crystal perfection was seen for the microgravity crystals. This analysis was later developed into an expression for anisotropic mosaicity in a study of microgravity crystal growth and impurity effects on lysozyme (Snell *et al* 2001).

$$\eta_{hkl}^{\text{calc}} = \left[\eta_{abc} \left(\frac{(ah)^2 + (bk)^2 + (cl)^2}{a^2 + b^2 + c^2} \right) + \eta_{def} \left(\frac{(dh)^2 + (ek)^2 + (fl)^2}{d^2 + e^2 + f^2} \right) \right.$$
$$\left. + \eta_{mno} \left(\frac{(mh)^2 + (nk)^2 + (ol)^2}{m^2 + n^2 + o^2} \right) \right] [h^2 + k^2 + l^2]^{-1} + \eta_{\text{const}}. \tag{8.3}$$

The mosaicity measured from the crystal is a global measure of several effects. Simple rocking curve measurements cannot separate effects arising from strain (i.e. lattice spacing variations) from those arising from the classical definition of mosaicity which involves only domain misalignment, see section 1.3. The separation requires that reciprocal space is mapped in two

dimensions. The technique used for this purpose is the triple-axis spectrometer first used for neutron scattering (Brockhouse 1955). The application of reciprocal space mapping to x-ray techniques is well described elsewhere (Fewster 1996, 1997). Boggon *et al* (2000) combined this with mosaicity and topography methods to look at microgravity and ground-grown crystals. Figure 16 shows the instrumental geometry used and an example of a reciprocal space map from a microgravity-grown lysozyme crystal.

The measurements described in the lysozyme studies were in themselves technique development and time consuming. The next step was the development of methods that allowed for a similar analysis but with a statistical number of samples now given in section 8.3.

8.3. Insulin: an example of physical and structural studies enabling statistical analysis

Insulin is a small protein hormone that controls glucose homeostasis by stimulating the uptake of glucose into skeletal muscle and, to a lesser extent, into liver and adipose tissue. Human insulin consists of 51 amino acids, divided into two chains, commonly labelled A and B, with 21 and 30 amino acids, respectively. Insulin used in the treatment of diabetes mellitus is prepared as a time released crystalline product. It is stored as a zinc-complexed hexamer and active in its monomeric form. Phenolic derivatives, by binding to the zinc-insulin hexamer in the crystalline state, retard the dissolution thereby slowing bioavailability and reducing a diabetic's injection frequency.

Recombinant insulin was crystallized in the PCF on Space Shuttle missions STS-57 and STS-60 (Long *et al* 1996). Crystallization took place by lowering the temperature from 40°C to 22°C over approximately 120 h. Insulin crystals from STS-57 mission were larger by a factor of 1.6 than their earth-grown counterparts, and were optically superior, i.e. had fewer flaws. The x-ray evaluation showed an increase in signal-to-noise over the entire diffraction resolution range. Similarly, crystals from the STS-60 mission were larger by a factor of two over the earth-grown counterparts and again were optically superior with fewer visible flaws. X-ray data also showed an increase in signal-to-noise over the entire resolution range and provided electron density maps with 1.4 Å resolution compared to 1.9 Å from earth-grown counterparts. The microgravity-grown crystals showed that two molecules of parahydroxybenzamide were bound in the complex (Smith *et al* 1996), a result that was unclear from the ground-grown crystal data.

Insulin crystals grown by the same method on the STS-86 mission, gave structural data to 1.0 Å resolution on a laboratory source (Smith *et al* 2003). Insulin undergoes a transition from its B chain extended (or taut structural state) to a helical conformation (relaxed structural state) of the chain, termed T and R states, respectively. This transition is a key to producing greater stability in insulin preparations allowing less frequent dosing of the patient. The high-resolution study enabled by the microgravity-grown crystals suggested a region in the centre of the aggregated hexamer structure that plays a significant role in the T–R state transition. The detail revealed in the study was just short of that required to observe a key hydrogen bond in the region and neutron diffraction techniques or yet higher x-ray resolution diffracting crystals will yet be needed to completely understand this transition.

Ferrer *et al* (1998) developed an algorithm and software for mosaic spread analysis from an area detector and this prompted the development of a technique using fine angular slicing to probe the mosaicity of a statistical number of reflections from both the microgravity and ground crystals (Bellamy *et al* 2000, Lovelace *et al* 2000, Borgstahl *et al* 2001). The first use of this technique was to look at microgravity samples of insulin which were crystallized on STS-95 (Borgstahl *et al* 2001). The resulting crystals were on average 34 times larger than the ground-grown crystals and had fewer visual flaws. X-ray data were collected on beamline 1–5
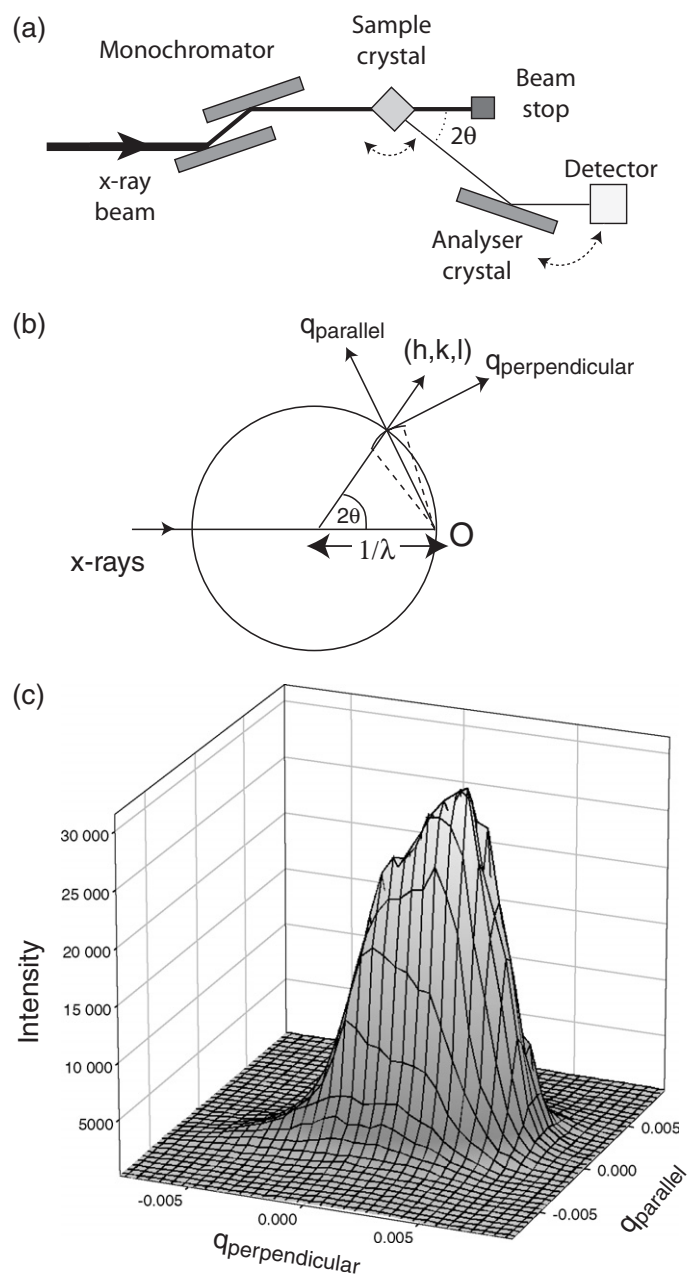
Figure 16. Reciprocal space mapping showing (*a*) instrumentation, (*b*) measurements in reciprocal space using the Ewald sphere construction and (*c*) the resulting reciprocal space map (Boggon *et al* 2000).

at Stanford Synchrotron Radiation Laboratory (SSRL). Between 447 and 502 reflections were profiled for each of six microgravity-grown insulin crystals. Between 14 and 174 reflections were profiled for equivalently accumulated data from six Earth crystals (the Earth crystals had weaker diffraction so it was not possible to collect as many reflections from them). The

crystals were not cryocooled. Data were processed using the BEAM-ish software (Lovelace *et al* 2000), specially developed for the study, to extract the mosaicity, η, using,

$$\eta = \frac{|\phi_{\mathrm{R}}| - \sqrt{L^2 \zeta^2 \gamma_{\mathrm{H}}^2 + \gamma_{\mathrm{V}}^2}}{(L\lambda/d)\cos\theta_{hkl}} - \left(\frac{\delta\lambda}{\lambda}\right)\tan\theta_{hkl}, \tag{8.4}$$

where, ϕ_R is the measured reflection width, ζ is the position of the corresponding reciprocal lattice point projected onto the rotation axis, d is the resolution ($d/n = \lambda/2\sin\theta_{hkl}$), η is the mosaic spread, γ_{H} and γ_{V} are the horizontal and vertical crossfire at the sample and L is the correction for the Lorentz effect (Greenhough and Helliwell 1982).

The best microgravity-grown insulin crystals had an average η of 0.002° with a standard deviation of only 0.001°. Two of the earth-grown crystals had fairly low mosaicity with average η values of 0.013° (s.d. 0.004°) and 0.017° (s.d. 0.005°), respectively, yet these η values were 6.5 and 8.5 times higher than the best microgravity crystals. Both the ground-grown crystals diffracted weakly compared to the microgravity-grown crystals. For any given Earth crystal, the η values for individual reflections varied over a surprisingly large range, with standard deviations of 0.004–0.024°. The spread in η for microgravity crystals was four- to five-fold narrower with standard deviations ranging from 0.001 to 0.005°. In a few cases, the best Earth η values overlap the worst microgravity values. This illustrates the importance of collecting a statistically significant number of reflections from each sample since an unlucky selection of a few reflections could lead to an erroneous conclusion. A non-parametric, distribution-free, Mann–Whitney rank sum test confirms that the microgravity and the Earth data were statistically different from each other at the 99% confidence interval.

De Mattei *et al* (2001) used laboratory x-ray diffraction techniques and light scattering tomography to study insulin crystals from the same mission. Light scattering tomography directly images defects in the crystal and identifies the character of those defects. X-ray data were only collected on one crystal of each sample and despite showing an improvement for the microgravity case is not as meaningful as the statistical study described above. Three crystals, one microgravity-grown and two ground-grown crystals were studied by tomography. A small number of spherical micro-defects were seen in the microgravity-grown crystals while the ground-grown crystals had such a large number of defects that single defects could not be isolated in some regions.

Typically, for structural biology purposes, crystals are cryocooled to reduce radiation damage associated with data collection at synchrotron x-ray sources. The effect of this cryocooling is to decrease the long-range order in the crystal resulting in an increase in the mosaic spread (Mitchell and Garman 1994, Rodgers 1994, Teng and Moffat 1998, Kriminski *et al* 2002). The insulin crystals described in Borgstahl *et al* (2001), that showed such a dramatic improvement from microgravity referred to above were studied at ambient temperatures, but were then also studied after cryocooling (Vahedi-Faridi *et al* 2003a). Cryocooling caused a 43-fold increase in mosaicity for the microgravity-grown crystals and an eight-fold increase for the ground-grown crystals (average 0.217° and 0.246°, respectively). Interestingly, the cryocooling did not cause the observable formation of any additional scattering domains in the crystals. Once the domains in the crystals have formed they stay, even during cryocooling. The microgravity-grown crystals had a reduced number of domains seen in the reflection profile and the mosaicity increase reduced the signal-to-noise of the reflections somewhat less than in the earth-grown case. The improved signal from the microgravity crystals along with the increased volume facilitated the measurement of weaker high-resolution reflections.

8.4. Improvements at the short-range, macromolecular structural level

Table 2 has listed a number of examples where microgravity crystals have produced increased resolution diffraction allowing enhanced *structural* knowledge to be obtained. In this section we give several case studies where the fine structural differences have been probed. Benchmarking of the effect of microgravity using a long-range order parameter like mosaicity is reasonably straightforward, once the apparatus and methods to probe very fine angular values on weakly diffracting crystals by x-rays have been mastered. Making detailed molecular structure comparisons is less easy as structures are determined by a large number of reflection intensity data and small differences in experimental protocol can lead to variations in the precision of the structure refinements which can seriously weaken a comparison-result. So, protocols have been developed to afford confident comparisons. These have included (i) using as closely similar crystal volumes as possible, (ii) as closely similar an x-ray measuring protocol as possible, (iii) working with common reflections between the crystals being compared, and finally (iv) using more than one software package to test the sensitivity of the final structure refined models to small changes in refinement technique. Given the effort involved it has not yet proved possible to investigate a large number of crystal structure refinements in two large population groups or to systematically vary the software at other stages of the analysis. To date there have been relatively few studies on these levels of molecular structure comparisons, but three examples can be given showing what can be achieved and how each reached a conclusion.

Dong *et al* (1999) undertook a comparative study of the bound-solvent structures for microgravity-, ground control-, gel- and microbatch-grown chicken egg-white lysozyme crystals at 1.8 Å resolution. The logic of this being that if the fluid state is more stable then perhaps an improvement might manifest itself in the bound solvent structure (Dong *et al* 1998). The microgravity crystals were grown in the APCF on STS-78, and as with the ground-controls by the dialysis method, crystallization in agarose gel used a tube liquid–gel diffusion method and crystallization in microbatch involved drops immersed under oil. X-ray data were collected using a laboratory-based CuKα rotating anode source and image plate detector. The lysozyme protein structures corresponding to these four different crystallization methods remained similar. A small improvement in the bound-solvent structure was seen in the lysozyme crystals grown in microgravity by dialysis. The improvements were manifest in terms of a small but significant increase in the number of bound water molecules found and the common waters had improved *B*-factors.

Ng *et al* (2002) studied the dimeric multidomain enzyme aspartyl-tRNA synthetase from *Thermus thermophilus* which was crystallized within dialysis reactors of the APCF in the laboratory on Earth and under microgravity. A comparison crystallographic analysis revealed that the crystals grown in microgravity were superior in every respect to control crystals prepared in otherwise identical conditions on Earth. The crystals diffracted x-rays more intensely (and had a lower mosaicity), facilitating the process of structure determination. Indeed, the electron-density map calculated from diffraction data of space-grown crystals contained considerably more detail. The resulting three-dimensional structure model at 2.0 Å resolution was more accurate than that produced in parallel using the data originating from earth-grown crystals. The major differences between the structures, included better defined amino-acid side chains and an improved order of bound water molecules.

Habash *et al* (2003) undertook protein structure refinements and electron-density map comparisons of apocrustacyanin C$_1$ crystals grown in microgravity and on Earth using vapour-diffusion geometry. Models of apocrustacyanin C$_1$ were refined against synchrotron x-ray data recorded to resolutions of 1.85 and 2 Å from a microgravity-grown and an earth-grown crystal, respectively, both using vapour-diffusion crystal-growth. The microgravity crystals

were grown in the APCF on the STS-78 mission. There was improved electron density found for some amino acid residue side chains; most interestingly these were on the surface of the protein with two involved in or nearby crystal lattice-forming interactions. This observation makes a link with an improved crystal-growth mechanism at the molecular level.

9. Limitations and ground-based alternatives

9.1. Limitations

Microgravity crystallization experiments have very specific limitations; getting the experiment into space, operating it there and then returning the samples once the experiment is complete. Another limitation is the time it takes to perform a successful microgravity experiment.

9.1.1. Time taken to iterate. Analysis of the results from microgravity experiments takes place when the samples have returned to Earth. Acting on those results to optimize the crystals further requires waiting for another launch. Between 1991, after the Challenger accident, and 2003, before the Columbia accident, the space shuttle averaged about six missions a year. To achieve a success rate of 60%, i.e. by flying four or more missions (Kundrot *et al* 2001), it would take an absolute minimum time period of 10 months after the first launch of the experiment until the optimum crystals were returned from the fourth flight. This assumes that the results will be analysed before the launch of the next mission, that sufficient sample is available for the next experiment, and the same apparatus is carried on subsequent missions. Thus, one can immediately see that in practice it takes time for the methods in the field to develop. The situation is somewhat worse with the ISS. Flights to the Space Station transfer experiments to the Space Station and then bring down experiments left from previous flights. The Orbiter is docked at the station for a limited time, some distance from the centre of mass. An acceleration noisy environment results from the transfer of equipment, experiments and supplies. Few if any experiments requiring microgravity can be performed on the Orbiter during this time. It is not possible to make use of sequential flights as the results are not known before the next mission launches. The time to get the best crystals is increased to over a year, at the very best, from the first experiment.

9.1.2. Before launch. Launching a spacecraft invariably involves a large quantity of propellant. In the case of the Space Shuttle once the external tank filling process starts there is no access to the experimental apparatus onboard. Solutions have to be loaded into the apparatus and the apparatus placed onboard several days before the planned launch. If the launch happens as planned, the experiments will be activated either after reaching orbit or once transferred to the Space Station. However, many things can cause the cancellation of a launch. In this case, depending on the cause and length of delay the samples may have to remain in the apparatus on the launch pad for several hours or days. Should the delay be significant an opportunity to refill the apparatus with fresh samples will be available. Each sample needs to be studied before the experiment to know what the effects of delays will have upon it and specifically to assess; how stable is the sample in solution, and if reloading opportunities present themselves should fresh sample be loaded? If the sample is sensitive then enough of the sample should be available for one or more reloading attempts as a precaution. Alternatively, a backup experiment should be available.

9.1.3. During the mission. The accelerations and disturbances associated with space flight have been discussed in section 3. Dedicated microgravity flights, i.e. those striving to maintain
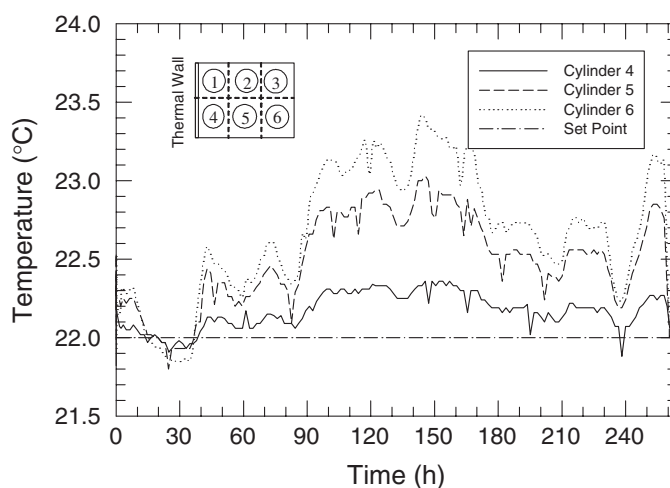
Figure 17. Temperature recorded for a row of PCAM cylinders inside a thermal enclosure controlled to a set point of 22°C. The cylinders are, closest (#4), mid-way (#5) and farthest away (#6) from the controlling wall.

the lowest possible acceleration environment, produce significantly better results than those where crystallization was a parasitic activity (Judge *et al* 2005). Maintaining a low acceleration environment is important. The experimenter has no control over the mission duration. For space shuttle missions there is some correlation between mission duration and success of experiments but the predominant factor was the acceleration environment (Judge *et al* 2005). There have, in practice, been very few such dedicated missions which exacerbates the time taken to make iterative developments, described above.

In the laboratory on the ground temperature can be controlled in an incubator with an accuracy better than ±1°C. Convective heat transfer is minimal in microgravity and heating or cooling during the mission has to be accomplished by conduction or forced air. As an example, figure 17 illustrates temperatures recorded in the STES system in three PCAM cylinders during the STS-95 mission. Temperature control is by conduction and the variation in temperature is a function of the distance of the cylinder from the controlling wall. The data show that the actual temperature close to the controlling wall is within 0.5°C of the set point, however peak deviations from the set point of 1.0°C in the middle cylinder and 1.5°C for the cylinder farthest away from the controlling wall are observed. Therefore the position of the sample within this thermal enclosure affects the temperature control experienced by the experiment. Other systems, such as the APCF, use forced air convection as part of the apparatus and achieve a temperature control better than ±0.1°C (Snyder *et al* 1991, Bosch *et al* 1992, Snell *et al* 1995). The temperature sensitivity of the experiment and the method of controlling temperature (which can be solved, e.g. as in the APCF) need to be considered for the success of the experiment.

9.1.4. Returning samples.   The return of samples is directly related to when the launch of the mission occurs. If the mission launch gets delayed then so will the return of samples. Landing for NASA Space Shuttle missions takes place in Florida (preferred for logistical reasons) or California. Good weather is needed and this is the critical factor in determining the actual landing time and location. The landing will not necessarily be at the date, time or place initially planned. The apparatus is unloaded from the Orbiter and transported to a laboratory where

the samples are photographed and distributed to the investigators. Landing for non-shuttle missions is currently by parachute and subject to weather delays and location uncertainty.

Any plan to perform rapid analysis of the crystals, e.g. at a synchrotron has to take into account potential delays from the planned date of return. Alternatively plans can be made to cryoprotect the crystals (Rodgers 1994, 1997, Garman and Schneider 1997) on their return for long-term storage. Cryoprotection is common for x-ray data collection at synchrotron sources but destroys some of the long-range order within the crystal, i.e. greatly increasing mosaicity (Vahedi-Faridi *et al* 2003a).

9.1.5. Prerequisites for samples.

9.1.5. Prerequisites for samples. When using NASA hardware a prerequisite for a flight has been to know crystallization conditions on the ground. There is no physical reason to suggest that reducing the level of acceleration should cause the biochemical conditions to shift to such an extent that crystals would form in microgravity where they did not previously in screening on the ground. However, if microscopic crystals, too small to be visible, had formed on the ground then reducing the acceleration would allow them to grow larger and perhaps become visible. To date, there is no published data on the results of screening a sample in microgravity in comparison to screening on the ground. With continuing developments in bioinformatics and an increased fundamental understanding of short-range improvements in microgravity it may become possible to predict those macromolecules expected to result in improved crystals.

Solutions, including all the biochemicals in the experiment, need to be non-hazardous. A spacecraft is a closed environment where any spills will remain and worse, those spills may float making it easy to breath in, ingest or get the material in the eye of an astronaut. Several levels of containment are used for experiments but before a sample can be used a worst case scenario is assumed. This sometimes makes it impossible to use the optimum ground developed conditions and limits the type and extent of samples that can be flown.

9.2. Alternative means to reduce convection and sedimentation

The degree of buoyancy-driven convection in a system is measured by the Grashof number, where,

$$Gr = a\frac{d\rho}{dc}\Delta c L^3 v^{-2},\tag{9.1}$$

where a is the acceleration, ρ is the fluid density, Δc is the difference in bulk and the interfacial solute concentration, L is a characteristic length and v is the kinematic viscosity ($v = \mu/\rho$ where μ is the viscosity). When $Gr \gg 1$, as in crystallization on the ground, buoyancy effects dominate the system. By conducting the experiment in orbit the acceleration, a, is reduced and hence the buoyancy-driven convection is minimized. By examination of equation (9.1) it becomes clear that there are other means of mimicing microgravity and reducing the buoyancy-driven convection, i.e. reducing the change of concentration with density, $d\rho/dc$, minimizing the dimensions, L, or increasing the viscosity μ. Reducing $d\rho/dc$ is difficult as macromolecules are very sensitive to small changes in biochemical conditions or temperature. Similarly, a related approach, designing the experiment such that density gradients inhibit rather than promote convection (Nerad and Shlichta 1986) is non-trivial for biological macromolecules. Two readily applicable approaches are the minimization of dimensions, e.g. with the use of capillary growth, small crystallization volumes and microfluidics, or increasing the viscosity of the system, e.g. with the use of crystallization in gels.

9.2.1. Minimizing dimensions. The gel acupuncture technique makes use of capillaries to grow crystals (Garcia-Ruiz 1994). The technique reduces the convective flux by use of small

characteristic dimensions, i.e. the capillary, and has a second advantage in that it has a long diffusional path length and narrow area of diffusion front. This gives a gradient of conditions along the capillary. Experimental results establishing the technique on the ground (Garcia-Ruiz 1994) showed that crystal nucleation density decreased and crystal volume increased with capillary length.

With the development of robotic technologies applied to structural genomics crystallization in very small solution volumes is now routine (Hosfield *et al* 2003, Weselak *et al* 2003). The volumes used are measured in nanolitres and there is evidence that there is a reduction in convection and increase in crystal quality (Carter *et al* 2005).

Microfluidics is a science that manipulates fluids on a microscopic scale. A wide variety of analyses and applications have already been developed using this technology (Verpoorte 2002). Macromolecular crystallography using microfluidics has been reviewed elsewhere (Hansen and Quake 2003, van der Woerd *et al* 2003). Microfluidic systems have a low Reynolds number, i.e. the ratio of force due to inertia and force due to viscosity. The flow is strictly laminar and mixing occurs only by diffusion. Hansen *et al* (2002) make use of a lab-on-a-chip for crystallization achieving a higher success rate than other standard laboratory techniques and the resulting crystals appearing faster. A slightly different approach was taken by Zheng *et al* (2004) who used microfluidic techniques to process and then fill solutions into a capillary for crystal growth external to the microfluidic device.

Nanovolume techniques and microfluidics are fairly recent technologies. It will remain to be seen if they will produce crystals of as high quality as the benchmark set by those from microgravity but equation (9.1) suggests there is every reason to think that this is possible.

9.2.2. Crystal growth in gels. Crystal growth in gels is well described by Robert and Lefaucheux (1988). The gels used for crystal growth are hydrogels having a liquid and solid phase. The solid phase is not a rigid network but made of entangled polymeric chains, e.g. gelatin or agarose, or cross-linked in the case of chemical gels, e.g. silica and polyacrylamide. Unlike solution crystal growth the crystals do not sediment but remain in the bulk of the gel supported by the gel network. The gel itself is trapped inside the crystal but is distributed randomly so no appreciable effect is seen in the diffraction (Gavira and Garcia-Ruiz 2002). Depletion zones are revealed around crystals growing in gels (Robert and Lefaucheux 1988).

Miller *et al* (1992) compared ground-based vapour diffusion, gel-growth and microgravity growth of human serum albumin crystals. Different gels were used with the best crystals produced in agarose gels as judged visually. Most importantly, x-ray data collection showed that the microgravity crystals displayed higher signal-to-noise than the gel grown crystals which were in turn better than the ground grown crystals. Both the gel and microgravity crystals were larger than those grown by standard vapour diffusion. If gels improve crystal quality on the ground what happens when a gel is used in microgravity? Lorber *et al* (1999) addressed this with a study crystallizing thaumatin in the APCF using agarose gel. Control experiments were conducted on the ground both in gel and solution. The crystals grown in gel, both on Earth and in microgravity were virtually identical in terms of their x-ray diffraction and differences in the crystals were marginal. Otalora *et al* (2001) showed that gels can provide a more uniform depletion zone than microgravity, albeit on a non-perfect, noisy microgravity mission.

9.2.3. Electromagnetic fields. Gels and microfluidics have been shown to reduce buoyancy-driven convection. In addition to reducing convection, crystal growth in gels also reduces

sedimentation. Another approach to reducing sedimentation is the use of electromagnetic fields.

A high magnetic field can produce a crystallization environment where the perceived acceleration can be reduced due to diamagnetic properties of the solutions used to grow a crystal (Wakayama *et al* 1997, Ramachandran and Leslie 2005, Saijo *et al* 2005). This both reduces sedimentation and damps convection. An 8–10 T magnetic field was used in the growth of snake muscle fructose-1,6-bisphosphatase and human estrogenic 17β-hydroxysteroid dehydrogenase crystals (Lin *et al* 2000). Both showed improved diffraction properties. The magnetic field is thought to affect the crystallization system by reducing the convection and delaying sedimentation. Mach–Zehnder interferometry studies of the growth of lysozyme crystals under a strong (6 T) magnetic field show a reduction in crystal growth rate but no effect on the convection or solubility (Yin *et al* 2001). Lysozyme crystal growth has been studied under differing magnetic field strengths, 11 T (opposing gravitational acceleration), 0 T, 15 T and 11 T (adding to gravitational acceleration) to provide microgravity, 1g, 1g with magnetic field, and 1.8g forces, respectively on the sample (Yin *et al* 2004). By reference to a standard crystal, the quality of the resulting crystals, measured by a relative Wilson plot (Arai *et al* 2004), was highest for the simulated microgravity (11 T) decreasing in the order, 1g (15 T), 1g (0 T) and finally the 1.8g (11 T) sample.

Another method used to mimic some of the aspects of microgravity crystal growth is electrostatic levitation. Electrostatic levitation for crystal growth (Rhim and Chung 1991) makes use of balancing,

$$mg = \frac{QV}{d},\tag{9.2}$$

where m is the sample mass which carries charge Q, and V is the voltage difference between electrodes and g is the acceleration due to gravity. On the ground the levitated drop size cannot exceed 90 μl (Rhim and Chung 1991) but experiments have been successful in growing crystals. A vapour diffusion experiment was set up using a drop of 18 μl total precipitant, protein and buffer and levitated with an initial voltage of 6.7 kV (Rhim and Chung 1991). Over time the levitated drop loses water through evaporation and the supersaturation increases. In this case three crystals formed in the drop with the largest crystal being 0.2 mm in the largest dimension. The authors propose the method as a means of vibrationally damping crystallization in microgravity which also allows much larger drops to be under controlled levitation. Although no x-ray work was carried out to study the resulting crystals visually they were indistinguishable from those grown in standard vapour diffusion setups.

9.3. Changing the macromolecule

In this review we have assumed that every condition on the ground has been optimized before resorting to growing a macromolecular crystal in microgravity. One aspect of the optimization that needs specific mention is the modification of the macromolecule itself using molecular biology methods. In general, the community that studies fundamental crystal growth has a different background to that interested in the structure and function of the macromolecule. There are then the powerful techniques of molecular biology to be considered. The macromolecule can be modified in many ways to increase the chance of obtaining crystals and to obtain improved crystals. Dale *et al* (2003) present a succinct review on these aspects. Complex formation and subsequent screening can be performed with co-factors, inhibitors or even antibody fragments. Enzymatic removal of sugars may help. Site directed mutagenesis, e.g. point mutations, N-terminal and C-terminal truncation or construction of fusion proteins can aid the process. Molecular biology techniques are now shown to be a valid approach to

getting the structure or improving current structural information. Being ground-based methods they are less expensive. Other reports on the successful use of molecular biology to enhance crystallization and the crystals themselves (especially their diffraction resolution) are presented elsewhere (Price and Nagai 1995, Derewenda 2004a, 2004b, McPherson 2004).

9.4. Methods for improving data quality from existing crystals

Besides improving the crystal growth environment or engineering of the macromolecule to enhance the data quality a number of methods have been used to enhance data from an already existing crystal.

The hydration state of the crystal can have significant effects on the quality of the resulting data. Hydration resolved diffraction patterns of DNA revealed the different conformers of DNA fibres (Franklin and Gosling 1953) that led to the double helix proposed model (Watson and Crick 1953) and which was steadily refined by Wilkins *et al* (1953). Apparatus to control the DNA fibre humidity developed by Rosalin Franklin proved then to be particularly important. More recently, a device to systematically control the hydration/dehydration of single protein crystals in an environmental cell has now been described by Kiefersauer *et al* (2000). This device uses capillary-free mounting of protein crystals. A controlled stream of air allows an accurate adjustment of the humidity at the crystal. Experiments and results for different crystal systems demonstrated the use of their method, also in combination with flash-cooling, to improve crystal order. There are examples of such (de)hydration resolved studies improving the protein crystal diffraction resolution. A chance event of steady dehydration of a HIV reverse transcriptase crystal improved the diffraction resolution from 3.7 to 2.2 Å (Esnouf *et al* 1998). Abergel (2004) reports spectacularly improved diffraction resolution of several macromolecules by dehydration methods.

Cryocrystallography (Hope 1988, Garman and Schneider 1997, Rodgers 1997, Garman 1999), i.e. vitrifying and maintaining the crystal at cryogenic temperatures, is used extensively to reduce x-ray radiation damage and to reduce thermal motion of the atoms resulting in improved data quality. Recently it has been introduced in macromolecular neutron crystallography (Blakeley *et al* 2004a, 2004b). Cryocooling has the disadvantage that it greatly reduces the long-range crystal quality resulting in a significant increase in the mosaicity (Mitchell and Garman 1994, Vahedi-Faridi *et al* 2003a). To mitigate this somewhat annealing methods have been developed where the crystal is warmed up after initial cryocooling then flash cooled again. This annealing shows promise in reducing this mosaicity and enhancing diffraction resolution (Harp *et al* 1998, 1999, Yeh and Hol 1998, Ellis *et al* 2002, Kriminski *et al* 2002, Hanson *et al* 2003a, 2003b) but does not come close to returning the long-range order to its original state.

Altering the hydration state and cryocrystallography studies cause some macromolecular structural change. This is tolerated in return for improved diffraction data and structure precision. Where considered critical structural studies at closer to physiological temperatures can also be conducted as an adjunct to the cryo or dehydrated structures (see, e.g. Deacon *et al* (1997), Juers and Matthews (2001)).

9.5. High acceleration crystal growth

We have considered crystal growth in a reduced acceleration environment and crystal growth on the ground. If reduced acceleration increases crystal quality then perhaps increasing acceleration will reduce the quality? Lenhoff *et al* (1997) describe a number of experiments carried out using ultracentrifugal crystallization and report their own theory and results with the

successful crystallization of catalase. When a solution is rotated in a centrifuge an equilibrium is established between random diffusion and the tendency of dense solute macromolecules to concentrate in the direction of the acceleration. A stable concentration gradient is formed. If the initial solution is near supersaturation the outer portions of the redistributed solution are supersaturated and crystal growth can occur. Aspartic proteinase was also crystallized by centrifugation at $3000g$ and the resulting single crystals gave diffraction data to $2.3\,\text{Å}$ (Pitts 1992); no comparison with crystals grown at unit gravity was made. Studies with small molecules, lead nitrate and potassium bromide, have been successful in forming single crystals at high acceleration (Shlichta and Knox 1968). The process causes submicroscopic particles to sediment, removes spurious growth at the solution surface, removes bubbles and minimizes convection as any solution changes are quickly damped by the density gradient. The disadvantages are that high forces can occur on the crystals.

10. Future directions and summary

Currently there are no techniques to predict why or if a crystal will improve from growth in microgravity. Extrapolating from the case of lysozyme Vekilov *et al* (1996) proposed that crystal quality can be increased by enhancing or suppressing the transport in solution. Based on Péclet numbers (expressed as the ratio of bulk mass transport and the crystal interface kinetics) calculated from kinetic data the authors predict that canavalin and Satellite Tobacco Mosaic Virus (STMV) (having a mixed growth regime) should show greater crystalline perfection in microgravity while thaumatin and lysozyme (having mostly kinetic dominated growth) would not be expected to show improvement. While trends contrary to Vekilov's theory are often observed (Vergara *et al* 2003, Judge *et al* 2005), these trends do not invalidate the theory. More extensive kinetic measurements of individual macromolecules and the crystallization process are needed to assess or improve its predicting power; the need for a good theoretical understanding is still a pressing need for the future.

The fundamentals of microgravity crystallization and how improved crystals result are not completely understood, however we know that improved quality crystals do result. In terms of long-range order, the resulting volume is increased and the mosaicity is decreased. This perfection can be harnessed (Blakeley *et al* 2004a, 2004b, Helliwell 2005). The larger crystal volume and reduced mosaicity have an immediate interest for neutron crystallography. A reduced mosaicity from microgravity-growth is also useful for samples where the mosaicity is currently too great to accurately record and integrate data from the samples. There is evidence that improvements may occur on the molecular, short-range order level. Resolution enhancements (table 2), small but significant differences in bound water structure (Dong *et al* 1999), and improved order at amino acid residues involved in protein to protein lattice interactions have also been seen (Ng *et al* 2002, Habash *et al* 2003). The reasons for these short-range improvements are not clear. Improved long-range order increasing the accuracy of reflection intensity measurement may be the explanation. Alternatively, a reduction in disorder diffuse scattering, i.e. pushing diffracted x-rays into the Bragg peaks, is also a possibility, corroborated by the small molecule example of Ahari *et al* (1997) but diffuse scattering reduction for macromolecular crystals is not systematically investigated as yet.

Microgravity crystallization has typically used apparatus developed around methods based in the terrestrial laboratory. Studies to understand the unique aspects of microgravity and the effect on the crystallization process have largely been parasitic aspects of the production of crystals for structural data collection. Apparatus purely for studying crystallization in microgravity has now been designed and built however. ESA's new Protein Crystallization Diagnostics Facility (PCDF) holds four individual samples with diagnostic instrumentation and

precise, active, thermal control (Pletser *et al* 1991, 2001). Based on experience with the APCF the PCDF uses a high-resolution video microscope, a dynamic light scattering system and a Mach–Zehnder interferometer. Another diagnostic apparatus is the observable protein crystal growth apparatus (OPCGA) (McPherson *et al* 1999). This employs fused optics, a video microscope and a phase shifting Mach–Zehnder interferometer to analyse the crystals and the fluid field around the crystals. Experiments on the ground have shown that depletion zones can be seen and measured around growing crystals (McPherson *et al* 1999). Such apparatus needs to be applied in future systematic investigations of the biophysical chemistry of macromolecular crystal growth in microgravity to further understand and optimize the use of microgravity.

Microgravity provides a useful tool to study the physics of crystal growth in a way that can be easily modelled and tested. Crystals that have resulted have set a benchmark for the quality that can be achieved. However, given the limited success rate and results to date, the cost–benefit of crystallization experiments in microgravity has been controversial (Leberman 1985, Naumann *et al* 1985, McPherson and DeLucas 1999). Financially, in 2004, the NASA/Air Force Cost Model (NAFCOM) estimates that it costs ∼$400k per kg to develop a human rated spacecraft and ∼$30k per kg to build the first example. The present launch costs to put a payload into space are on the order of $10k per kg. The space shuttle (Orbiter, solid rocket boosters and external tank) have a launch mass of approximately 2 million kg and a payload capacity of approximately 20 000 kg. Most of the crystallization apparatus described in sections 5 and 6 are designed to fit into a Space Shuttle Orbiter middeck locker which holds just under 25 kg. Using this as an upper limit this gives a cost to develop new apparatus of about $10M, about $750k to build it and then $250k to fly it each time. If we take the example of PCAM (Carter *et al* 1999b) with 378 individual experiments we get a cost for a single flight of about $27k per crystallization experiment. Using the same apparatus over 10 flights breaks down to a cost of about $3500 per single experimental growth condition, or about $175k for 50 conditions.

Crystallization in microgravity is financially expensive, but not astronomically so. We also have to consider the human cost of manned spaceflight. The current microgravity crystallization apparatus is highly automated and requires minimal astronaut input—in fact accelerations from astronaut activity and other sources actually reduce the overall success rate (Judge *et al* 2005). The EURECA satellite was successful in producing a quiet environment for crystal growth and this may well be the direction to take in the future. A free-flying, unmanned facility does not have to be large or prohibitively expensive and can be launched on an unmanned vehicle. The crystals remain in a fluid such that they can withstand the same re-entry forces that astronauts do on their return to the ground. Given the advances in robotic technologies developed for structural genomics and telescience techniques it is easily conceivable that iterative science could be performed. Optimizing the crystals could take place remotely with the best samples then returned to the ground for diffraction analysis. This approach removes many of the limiting factors described in section 9.1.

Developments on the ground, i.e. nanovolume crystallization and microfluidics, offer the potential to provide some of the advantages of microgravity growth. Growing large, well-ordered crystals, is still a significant ability for microgravity and its use may well see a resurgence with the demand for large samples in the growing neutron crystallography field.

In this review we have presented the basics of macromolecular crystallography and explained why microgravity has been an environment used for crystallization. Our own approach to this research area has been guided by choosing to study the changes to the order of crystals both physically and structurally. There is a great deal of physics involved with microgravity crystallization, some of it known, and undoubtedly much yet to discover.

Acknowledgments

References

Abergel C 2004 *Acta Crystallogr. D Biol. Crystallogr.* **60** 1413–6
Ahari H *et al* 1997 *Nature* **388** 857–60
Alvarado U R, DeWitt C R, Shultz B B, Ramsland P A and Edmundson A B 2001 *J. Cryst. Growth* **223** 407–14
Andrews S J, Hails J E, Harding M M and Cruickshank D W J 1987 *Acta Crystallogr.* A **43** 70–3
Arai S, Chatake T, Suzuki N, Mizuno H and Niimura N 2004 *Acta Crystallogr. D: Biol. Crystallogr.* **60** 1032–9
Authier A 2003 Dynamical theory of x-ray diffraction *IUCr Monographs on Crystallography* (Oxford: Oxford University Press)
Barnes C L, Snell E H and Kundrot C E 2002 *Acta Crystallogr. D: Biol. Crystallogr.* **58** 751–60
Bartels W J 1983 *J. Vac. Sci. Technol.* B **1** 338–45
Bellamy H D, Snell E H, Lovelace J, Pokross M and Borgstahl G E 2000 *Acta Crystallogr. D: Biol. Crystallogr.* **56** 986–95
Bergfors T M 1999 *Protein Crystallization* International University Line
Berisio R, Vitaglinao L, Mazzarella L and Zagari A 2002 *Protein Sci.* **11** 262–70
Betzel C, Gourinath S, Kumar P, Kaur P, Perbandt M, Eschenburg S and Singh T P 2001 *Biochemistry* **40** 3080–8
Blakeley M P, Cianci M, Helliwell J R and Rizkallah P J 2004a *Chem. Soc. Rev.* **33** 548–57
Blakeley M P, Kalb A J, Helliwell J R and Myles D A 2004b *Proc. Natl Acad. Sci. USA* **101** 16405–10
Blow D 2002 *Outline of Crystallography for Biologists* (Oxford: Oxford University Press)
Boggon T J *et al* 1998 *Phil. Trans. R. Soc. Lond.* A **356** 1045–61
Boggon T J, Helliwell J R, Judge R A, Olczak A, Siddons D P, Snell E H and Stojanoff V 2000 *Acta Crystallogr. D: Biol. Crystallogr.* **56** 868–80
Borgstahl G E O, Vahedi-Fardi A, Lovelace J, Bellamy H and Snell E H 2001 *Acta Crystallogr. D: Biol. Crystallogr.* **57** 1204–7
Bosch R, Lautenschlager P, Potthast L and Stapelmann J 1992 *J. Cryst. Growth* **122** 310–16
Brockhouse B N 1955 *Phys. Rev.* **99** 601–3
Broutin-L'Hermite I, Ries-Kautt M and Ducruix A 2000 *Acta Crystallogr. D: Biol. Crystallogr.* **56** 376–8
Buerger M J 1980 *X-Ray Crystallography* (Huntington, NY: Robert E Krieger)

Cang H-X and Bi R C 2001 *J. Cryst. Growth* **232** 473–80

Carter D C, Rhodes P, McRee D E, Tari L W, Dougan D R, Snell G, Abola E and Stevens R C 2005 *J. Appl. Cryst.* **38** 87–90

Carter D C *et al* 1999a *J. Cryst. Growth* **196** 602–9

Carter D C *et al* 1999b *J. Cryst. Growth* **196** 610–22

Castagnolo D, Carontenuto L, Vergara A, Paduano L and Sartorio R 2001 *J. Cryst. Growth* **232** 138–48

Chayen N E 1998 *Acta Crystallogr. D: Biol. Crystallogr.* **54** (Pt 1) 8–15

Chayen N E 2004 *Curr. Opin. Struct. Biol.* **14** 577–83

Chayen N E *et al* 1996 *Q. Rev. Biophys.* **29** 227–78

Chayen N E, Snell E H, Helliwell J R and Zagalsky P F 1997 *J. Cryst. Growth* **171** 219–25

Chen P S, Shlichta P J, Wilcox W R and Lefever R A 1979 *J. Cryst. Growth* **47** 43–60

Chernov P G and Chernov A A 2002 *Solid State Phys.* **57** 1–147

Ciszak E, Hammons A S and Hong Y S 2002 *Cryst. Growth Des.* **2** 235–8

Colapietro M, Cappuccio G, Marciante C, Pifferi A, Spagna R and Helliwell J R 1992 *J. Appl. Cryst.* **25** 192–4

Dale G E, Oefner C and D'Arcy A 2003 *J. Struct. Biol.* **142** 88–97

Darwin C G 1922 *Phil. Mag.* **43** 800–29

De Mattei R C, Feigelson R S, Bray T L, DeLucas L J and Symersky J 2001 *J. Cryst. Growth* **232** 511–19

Deacon A, Gleichmann T, Kalb A J, Price H, Raftery J, Bradbrook G, Yariv J and Helliwell J R 1997 *Faraday Trans.* **93** 4305–12

Declercq J P, Evrard C, Lamzin V and Parello J 1999 *Protein Sci.* **8** 2194–204

DeLombard R, Finley B D and Baugher C R 1992 *AIAA J.* **92-0354** 1–10

DeLombard R, McPherson K, Moskowitz M E and Hrovat K 1997 Comparison tools for assessing the microgravity environment of missions, carriers and conditions *Technical Memorandum* (NASA)

DeLucas L *et al* 1994 *J. Cryst. Growth* **135** 183–95

DeLucas L 1986 *J. Cryst. Growth* **76** 681–93

DeLucas L J, Smith C D, Smith H W, Vijay-Kumar S, Senadhi S E, Ealick S E, Carter D C, Snyder R S, Weber P C and Salemme F R 1989 *Science* **246** 651–4

DeLucas L J *et al* 1991 *J. Cryst. Growth* **110** 302–11

Derewenda Z S 2004a *Structure (Camb)* **12** 529–35

Derewenda Z S 2004b *Methods* **34** 354–63

Dobrianov I, Finkelstein K D, Lemay S G and Thorne R E 1998 *Acta Crystallogr. D: Biol. Crystallogr.* **54** 922–37

Dong J, Boggon T J, Chayen N E, Raftery J, Bi R C and Helliwell J R 1999 *Acta Crystallogr. D: Biol. Crystallogr.* **55** 745–52

Dong J, Pan J, Wang Y and Bi R 1998 *Space Med. Med. Eng. (Beijing)* **11** 26–9

Drenth J 1999 *Principles of Protein X-ray Crystallography* (Berlin: Springer)

Ducruix A and Giege R (ed) 1999 *Crystallization of Nucleic Acids and Proteins. A Practical Approach* (Oxford: Oxford University Press)

Eilers D and Stark H R 1993 EURECA microgravity environment—preliminary flight data *CP* (NASA) pp 869–91

Eisenberg D 2003 *Proc. Natl Acad. Sci. USA* **100** 11207–10

Ellis M J, Antonyuk S and Hasnain S S 2002 *Acta Crystallogr. D: Biol. Crystallogr.* **58** 456–8

Ellison G, Ahmadi G, Regel L and Wilcox W 1995 *Micrograv. Sci. Technol.* **VIII** 140–7

Esnouf R M, Ren J, Garman E F, Somers D O, Ross C K, Jones E Y, Stammers D K and Stuart D I 1998 *Acta Crystallogr. D: Biol. Crystallogr.* **54** (Pt 5) 938–53

Esposito L, Sica F, Raia C A, Giordano A, Rossi M, Mazzarella L and Zagari A 2002 *J. Mol. Biol.* **318** 463–77

Evrard C, Fastrez J and Declercq J P 1998 *J. Mol. Biol.* **276** 151–64

Ferre-D'Amare A R and Burley S K 1994 *Structure* **2** 357–9

Ferrer J-L and Roth M 1998 *J. Appl. Cryst.* **33** 433–6

Fewster P F 1996 Reciprocal space mapping *X-Ray and Neutron Diffraction Dynamical Diffraction: Theory and Applications* vol 357, ed A Authier *et al* (New York: Plenum) pp 269–87

Fewster P F 1997 *Crit. Rev. Solid State Mater. Sci.* **22** 69–110

Fourme R, Ducruix A, Ries-Kautt M and Capelle B 1995 *J. Synchrotron Radiat.* **2** 136–42

Fourme R, Ducruix A, Ries-Kautt M and Capelle B 1999 *J. Cryst. Growth* **196** 535–45

Franklin R E and Gosling R G 1953 *Nature* **172** 156–7

Garcia Ruiz J M and Otalora F 1997 *J. Cryst. Growth* **182** 155–67

Garcia Ruiz J M, Otalora F, Novella M L, Gavira J A, Sauter C and Vidal O 2001 *J. Cryst. Growth* **232** 149–55

Garcia Ruiz J M 1994 *Acta Crystallogr. D: Biol. Crystallogr.* **50** 484–90

Garman E 1999 *Acta Crystallogr. D: Biol. Crystallogr.* **55** 1641–53

Garman E F and Schneider T R 1997 *J. Appl. Cryst.* **30** 211–37

Gavira J A and Garcia-Ruiz J M 2002 *Acta Crystallogr. D: Biol. Crystallogr.* **58** 1653–6

Giachetti E, Ranaldi F, Fiusco A, Tacconi M, Veratti R, Falciani P and Vanni P 1999 *Micrograv. Sci. Technol.* **12** 36–40

Giacovazzo C 2002 Fundamentals of crystallography *IUCr Texts on Crystallography* (Oxford: Oxford University Press)

Glover I D, Harris G W, Helliwell J R and Moss D S 1991 *Acta Crystallogr.* B **47** 960–8

Grant M L and Saville D A 1991 *J. Cryst. Growth* **108** 8–18

Grant M L and Saville D A 1995 *J. Cryst. Growth* **153** 42–54

Greenhough T J and Helliwell J R 1982 *J. Appl. Cryst.* **15** 338–51

Habash J, Boggon T J, Raftery J, Chayen N E, Zagalsky P F and Helliwell J R 2003 *Acta Crystallogr. D: Biol. Crystallogr.* **59** 1117–23

Hansen C L and Quake S R 2003 *Curr. Opin. Struct. Biol.* **13** 538–44

Hansen C L, Skordalakes E, Berger J M and Quake S R 2002 *Proc. Natl Acad. Sci. USA* **99** 16531–6

Hanson B L, Harp J M and Bunick G J 2003a *Methods Enzymol.* **368** 217–35

Hanson B L, Schall C A and Bunick G J 2003b *J. Struct. Biol.* **142** 77–87

Harp J M, Hanson B L, Timm D E and Bunick G J 1999 *Acta Crystallogr. D: Biol. Crystallogr.* **55** (Pt 7) 1329–34

Harp J M, Hanson B L, Timm D E and Bunick G J 2000 *Acta Crystallogr. D: Biol. Crystallogr.* **56** 1513–34

Harp J M, Timm D E and Bunick G J 1998 *Acta Crystallogr. D: Biol. Crystallogr.* **54** 622–8

He X M and Carter D C 1992 *Nature* **358** 209–15

Hedman B, Hodgson K O, Helliwell J R, Liddington R and Papiz M Z 1985 *Proc. Natl Acad. Sci. USA* **82** 7604–7

Helliwell J R 1988 *J. Cryst. Growth* **90** 259–72

Helliwell J R 1992 *Macromolecular Crystallography with Synchrotron Radiation* (Cambridge: Cambridge University Press) (reprinted in paperback 2005)

Helliwell J R 2005 *Acta Crystallogr. D: Biol. Crystallogr.* at press

Helliwell J R, Snell E and Weisgerber S 1996 An investigation of the perfection of lysozyme crystals grown in microgravity and on earth *Lecture Notes in Physics* vol 464, ed L Ratke *et al* (Heidelberg: Springer) pp 155–70

Helliwell J R, Snell E H, Chayen N E, Judge R A, Boggon T J and Pusey M L 2002 Fluid physics and macromolecular growth in microgravity *Physics of Fluids In Microgravity* ed R Monti (London: Taylor and Francis)

Hope H 1988 *Acta Crystallogr.* B **44** 22–6

Hosfield D, Palan J, Hilgers M, Scheibe D, McRee D E and Stevens R C 2003 *J. Struct. Biol.* **142** 207–17

Hu Z W, Thomas B R and Chernov A A 2001 *Acta Crystallogr. D: Biol. Crystallogr.* **57** 840–6

Judge R A, Snell E H and van der Woerd M 2005 *Acta Crystallogr. D: Biol. Crystallogr.* **61** at press

Juers D H and Matthews B W 2001 *J. Mol. Biol.* **311** 851–62

Jules K, McPherson K, Hrovat K and Kelly E 2004a *Acta Astronaut.* **55** 855–87

Jules K, McPherson K, Hrovat K, Kelly E and Reckart T 2004b *Acta Astronaut.* **55** 335–64

Kawaji M, Gamache O, Hwang D H, Ichikawa N, Viola J P and Sygusch J 2003 *J. Cryst. Growth* **258** 420–30

Kiefersauer R, Than M E, Dobbek H, Gremer L, Melero M, Strobl S, Dias J M, Soulimane T and Huber R 2000 *J. Appl. Cryst.* **33** 1223–30

Klukas O, Schubert W-D, Jordan P, Kraub N, Fromme P, Witt H T and Saenger W 1999 *J. Biol. Chem.* **11** 7351–60

Ko T-P, Day J, Malkin A J and McPherson A 1999 *Acta Crystallogr. D: Biol. Crystallogr.* **55** (Pt 8) 1383–94

Ko T-P, Kuznetsov Y G, Malkin A J, Day J and McPherson A 2001 *Acta Crystallogr. D: Biol. Crystallogr.* **57** 829–39

Koszelak S, Day J, Leja C, Cudney R and McPherson A 1995 *Biophys. J.* **69** 13–19

Koszelak S, Leja C and McPherson A 1996 *Biotechnol. Bioeng.* **52** 449–58

Kranspenharr R, Rypniewski W, Kalkura N, Moore K, DeLucas L, Stoeva S, Mikhailov A, Voelter W and Betzel C 2002 *Acta Crystallogr. D: Biol. Crystallogr.* **58** 1704–7

Kriminski S, Caylor C L, Nonato M C, Finkelstein K D and Thorne R E 2002 *Acta Crystallogr. D: Biol. Crystallogr.* **58** 459–71

Kundrot C E, Judge R A, Pusey M L and Snell E H 2001 *Cryst. Growth Des.* **1** 87–99

Larson M A 1991 *Advances in Industrial Crystallization* ed J Garside *et al* (Oxford: Butterworth-Heinemann) pp 20–30

Larson S B, Day J, Greenwood A and McPherson A 1998 *J. Mol. Biol.* **277** 37–59

Leberman R 1985 *Science* **230** 373–5

Lenhoff A M, Pjura P E, Dilmore J G and Godlewski J T S 1997 *J. Cryst. Growth* **180** 113–26

Lin H, Rosenberger F, Alexander J I D and Nadarajah A 1995 *J. Cryst. Growth* **151** 153–62

Lin S-X, Zhou M, Azzi A, Xu G-J, Wakayama N I and Ataka M 2000 *Biochem. Biophys. Res. Commun.* **275** 274–8

Littke W and John C 1984 *Science* **225** 203–4

Littke W and John C 1986 *J. Cryst. Growth* **76** 663–72

Long M M, Bishop J B, Nagabhushan T L, Reichert P, Smith G D and DeLucas L J 1996 *J. Cryst. Growth* **168** 233–43

Long M M *et al* 1994 *Microgravity Sci. Technol.* **7** 196–202

Lorber B, Ng J D, Lautenschlager P and Giege R 2000 *J. Cryst. Growth* **208** 665–77

Lorber B, Sauter C, Robert M C, Capelle B and Giege R1999 *Acta Crystallogr. D: Biol. Crystallogr.* **55** 1491–4

Lorber B, Theobald-Dietrich A, Charron C, Sauter C, Ng J D, Zhu D W and Giege R 2002 *Acta Crystallogr. D: Biol. Crystallogr.* **58** 1674–80

Lovelace J, Snell E H, Pokross M, Arvai A S, Nielsen C, Xuong N-H, Bellamy H D and Borgstahl G E O 2000 *J. Appl. Cryst.* **33** 1187–8

Matsumoto S and Yoda S J 1999 *J. Appl. Phys.* **85** 8131–6

Matthews B W 1968 *J. Mol. Biol.* **33** 491–7

McPherson A 1996 *Crystallogr. Rev.* **6** 157–308

McPherson A 1999 *Crystallization of Biological Macromolecules* (New York: Cold Spring Harbor Laboratory)

McPherson A 2004 *J. Struct. Funct. Genomics* **5** 3–12

McPherson A and DeLucas L 1999 *Science* **283** 1455

McPherson A, Greenwood A and Day J 1991 *Adv. Space Res.* **11** 343–56

McPherson A, Malkin A J, Kuznetsov Y G, Loszelak S, Wells M, Jenkins G, Howard J and Lawson G 1999 *J. Cryst. Growth* **196** 572–86

Miele A E, Federici L, Sciara G, Draghi F, Brunori M and Vallone B 2003 *Acta Crystallogr. D: Biol. Crystallogr.* **59** 982–8

Mikol V, Hirsch E and Giege R 1990 *J. Mol. Biol.* **213** 187–95

Miller T Y, He X-M and Carter D C 1992 *J. Cryst. Growth* **122** 306–9

Mitchell E P and Garman E F 1994 *J. Appl. Cryst.* **27** 1070–74

Monti R (ed) 2001 *Physics of Fluids in Microgravity* (London: Taylor and Francis)

Nadarajah A, Rosenberger F and Alexander J I D 1990 *J. Cryst. Growth* **104** 218–32

Nardini M, Spano S, Cericola C, Pesce A, Damonte G, Luini A, Corda D and Bolognesi M 2002 *Acta Crystallogr. D: Biol. Crystallogr.* **58** 1068–70

Naumann R J, Snyder R S, Bugg C E, DeLucas L J and Suddath F L 1985 *Science* **230** 375–6

Nave C 1998 *Acta Crystallogr. D: Biol. Crystallogr.* **54** 848–53

Nerad B A and Shlichta P J 1986 *J. Cryst. Growth* **75** 591

Ng J D, Lorber B, Giege R, Koszelak S, Day J, Greenwood A and McPherson A 1997 *Acta Crystallogr. D: Biol. Crystallogr.* **53** 724–33

Ng J D, Sauter C, Lorber B, Kirkland N, Arnez J and Giege R 2002 *Acta Crystallogr. D: Biol. Crystallogr.* **58** 645–52

Otalora F, Garcia Ruiz J M, Garvira J A and Capelle B 1999a *J. Cryst. Growth* **196** 546–58

Otalora F, Novella M L, Gavira J A, Thomas B R and Garcia Ruiz J M 2001 *Acta Crystallogr. D: Biol. Crystallogr.* **57** 412–7

Otaora F, Novella M L, Rondon D and Garcia Ruiz J M 1999b *J. Cryst. Growth* **196** 649–64

Pechkova E and Nicolini C 2004a *J. Cell Biochem.* **91** 1010–20

Pechkova E and Nicolini C 2004b *Trends Biotechnol.* **22** 117–22

Perutz M F 1992 *Protein Structure: New Approaches to Disease and Therapy* (New York: Freeman)

Pitts J E 1992 *Nature* **356** 392

Plass-Link A 1990 *Proc. 7th European Symp. on Materials and Fluid Sciences in Microgravity* (Noordwijk, The Netherlands: European Space Agency) pp 41–4

Pletser V, Minster O, Bosch R, Potthast L and Stapelmann J 2001 *J. Cryst. Growth* **232** 439–49

Pletser V, Stapelmann J, Potthast L and Bosch R 1999 *J. Cryst. Growth* **196** 638–48

Price S R and Nagai K 1995 *Curr. Opin. Biotechnol.* **6** 425–30

Pusey M L and Naumann R 1986 *J. Biol. Chem.* **261** 6524–29

Pusey M L, Witherow W and Naumann R 1988 *J. Cryst. Growth* **90** 105–11

Qi J and Wakayama N I 2000 *J. Cryst. Growth* **219** 465–76

Ramachandran N, Baugher C R and Naumann R J 1995 *Micrograv. Sci. Technol.* **VIII** 170–9

Ramachandran N and Leslie F W 2005 *J. Cryst. Growth* **274** 297–306

Rhim W-K and Chung S K 1991 *J. Cryst. Growth* **110** 293–301

Ries-Kautt M *et al* 1997 *J. Cryst. Growth* **181** 79–96

Robert M C and Lefaucheux F 1988 *J. Cryst. Growth* **90** 358–67

Rodgers D W 1994 *Structure* **2** 1135–40

Rodgers D W 1997 Practical cryocrystallography *Macromolecular Crystallography* vol 276 (part B) ed C W J Carter and R M Sweet (New York: Academic) pp 183–203

Rossmann M G and Arnold E (ed) 2001 *Crystallography of Biological Macromolecules International Tables for Crystallography* (Dordrecht: Kluwer)

Saijo S Y Y, Sato T, Tanaka N, Matsui T, Sazaki G, Nakajima K and Matsuura Y 2005 *Acta Crystallogr. D: Biol. Crystallogr.* **61** at press

Savino R and Monti R 1996 *J. Cryst. Growth* **165** 308–18

Savino R, Paterna D and Favaloro N 2002 *J. Thermophys. Heat Transfer* **16** 562–74

Schmidt H P, Koerver W and Patz B 1992 *J. Cryst. Growth* **122** 317–22

Shaikevitch A and Kam Z 1981 *Acta Crystallogr.* A **37** 871–5

Shlichta P J 1986 *J. Cryst. Growth* **76** 656–62

Shlichta P J and Knox R E 1968 *J. Cryst. Growth* **3** 808–13

Skinner R, Abrahams J P, Whisstock J C, Lesk A M, Carrell R W and Wardell M R 1997 *J. Mol. Biol.* **266** 601–9

Smith G D, Ciszak E and Pangborn W 1996 *Protein Sci.* **5** 1502–11

Smith G D, Pangborn W A and Blessing R H 2003 *Acta Crystallogr. D: Biol. Crystallogr.* **59** 474–82

Snell E H 1995 Uses of the synchrotron x-ray Laue technique and investigation of microgravity crystal growth *Chemistry, PhD Thesis* University of Manchester, p 296

Snell E H, Boggon T J, Helliwell J R, Moskowitz M E and Nadarajah A 1997a *Acta Crystallogr. D: Biol. Crystallogr.* **53** 747–55

Snell E H, Borgstahl G E and Bellamy H 2003 Macromolecular crystal quality *Macromolecular Crystallography* vol 368 (part C), ed R M Sweet and C W Carter Jr, pp 268–88

Snell E H, Cassetta A, Helliwell J R, Boggon T J, Chayen N E, Weckert E, Hölzer K, Schroer K, Gordon E J and Zagalsky P F 1997b *Acta Crystallogr. D: Biol. Crystallogr.* **53** 231–9

Snell E H *et al* 2001 *Cryst. Growth Des.* **1** 151–8

Snell E H, Weisgerber S, Helliwell J R, Weckert E, Hölzer K and Schroer K 1995 *Acta Crystallogr. D: Biol. Crystallogr.* **51** 1099–102

Snyder R S, Fuhrmann K and Walter H U 1991 *J. Cryst. Growth* **110** 333–8

Stavrinidis C, Stark H, Eilers D and Hornung E 1991 *Micrograv. Sci. Technol.* **III** 191–203

Stoddard B L, Strong R K, Farber G K, Arrott A and Petsko G A 1991 *J. Cryst. Growth* **110** 312–16

Stojanoff V and Siddons D P 1996 *Acta Crystallogr.* A **52** 498–99

Stojanoff V, Siddons D P, Monaco L A, Vekilov P and Rosenberger F 1997 *Acta Crystallogr. D: Biol. Crystallogr.* **53** 588–95

Stojanoff V, Siddons D P, Snell E H and Helliwell J R 1996 *Synchrotron Radiat. News* **9** 25–6

Symersky J, Devedjiev Y, Moore K, Brouillette C and DeLucas L 2002 *Acta Crystallogr. D: Biol. Crystallogr.* **58** 1138–46

Teng T Y and Moffat K 1998 *J. Appl. Crystallogr.* **31** 252–7

Terzyan S S, Bourne C R, Ramsland P A, Bourne P C and Edmundson A B 2003 *J. Mol. Recogn.* **16** 83–90

Trakhanov S D, Grebenko A I, Shirokov V A, Gudkov A V, Egorov A V, Barmin I N, Vainstein B K and Spirin A S 1991 *J. Cryst. Growth* **110** 317–21

Vahedi-Faridi A, Lovelace J, Bellamy H D, Snell E H and Borgstahl G E 2003a *Acta Crystallogr. D: Biol. Crystallogr.* **59** 2169–82

Vahedi-Faridi A, Porta J and Borgstahl G E 2003b *Acta Crystallogr. D: Biol. Crystallogr.* **59** 385–8

Vallazza M, Banumathi S, Perbandt M, Moore K, DeLucas L, Betzel C and Erdmann V A 2002 *Acta Crystallogr. D: Biol. Crystallogr.* **58** 1700–3

van der Woerd M, Ferree D and Pusey M 2003 *J. Struct. Biol.* **142** 180–7

Vekilov P, Alexander J I D and Rosenberger F 1996 *Phys. Rev.* E **54** 6650–60

Vergara A, Lorber B, Zagari A and Giege R 2003 *Acta Crystallogr. D: Biol. Crystallogr.* **59** 2–15

Verpoorte E 2002 *Electrophoresis* **23** 677–712

Volz H M and Matyi R J 1999 *Phil. Trans. R. Soc. Lond.* A **357** 2789–99

Volz H M and Matyi R J 2000 *Acta Crystallogr. D: Biol. Crystallogr.* **56** 881–9

Volz H M and Matyi R J 2001 *J. Cryst. Growth* **232** 502–10

Wakayama N I, Ataka M and Abe H 1997 *J. Cryst. Growth* **178** 653–6

Watson J D and Crick F H 1953 *Nature* **171** 737–8

Weisgerber S and Helliwell J R 1993 *Joint CCP4 + ESF-EAMCB Newsletter on Protein Crystallogr.* **29** 10–3

Weiss M S 2001 *J. Appl. Crystallogr.* **34** 130–5

Welberry T R 2004 Diffuse x-ray scattering and models of disorder *IUCr Monographs on Crystallography* (Oxford: Oxford University Press)

Weselak M, Patch M G, Selby T L, Knebel G and Stevens R C 2003 *Methods Enzymol.* **368** 45–76

Wilkins M H, Stokes A R and Wilson H R 1953 *Nature* **171** 738–40

Wilson A J C 1942 *Nature* **150** 151–2

Wilson K P 1995 *Acta Crystallogr. D: Biol. Crystallogr.* **51** 511–21

Wlison W W 1990 *Methods* **1** 110–17

Yeh J I and Hol W G J 1998 *Acta Crystallogr. D: Biol. Crystallogr.* **54** 479–80

Yin D, Inatomi Y and Kuribayashi K 2001 *J. Cryst. Growth* **226** 534–42

Yin D C, Wakayama N I, Harata K, Fujiwara M, Kiyishi T, Wada H, Niimura N, Arai S, Huang W D and Tanimoto Y 2004 *J. Cryst. Growth* **270** 184–91

Zagalsky P F, Wright C E and Parsons M 1995 *Adv. Space Res.* **16** 91–4

Zheng B, Tice J D, Roach L S and Ismagilov R F 2004 *Angew. Chem. Int. Ed. Engl.* **43** 2508–11